HHS Public Access

Author manuscript

Inhal Toxicol. Author manuscript; available in PMC 2023 January 30.

Published in final edited form as:

Inhal Toxicol. 2022 ; 34(7-8): 200–218. doi:10.1080/08958378.2022.2081386.

Pulmonary toxicity and gene expression changes in response to whole-body inhalation exposure to multi-walled carbon nanotubes in rats

Tina M. Sager,

Christina M. Umbright,

Gul Mehnaz Mustafa,

Jenny R. Roberts,

Marlene S. Orandle,

Jared L. Cumpston,

Walter G. McKinney,

Theresa Boots,

Michael L. Kashon,

Pius Joseph

Health Effects Laboratory Division, National Institute for Occupational Safety and Health (NIOSH), Morgantown, WV, USA

Abstract

Purpose: To investigate the molecular mechanisms underlying the pulmonary toxicity induced by exposure to one form of multi-walled carbon nanotubes (MWCNT-7).

Materials and methods: Rats were exposed, by whole-body inhalation, to air or an aerosol containing MWCNT-7 particles at target cumulative doses (concentration × time) ranging from 22.5 to 180 (mg/m^3)h over a three-day (6 hours/day) period and toxicity and global gene expression profiles were determined in the lungs.

Results: MWCNT-7 particles, associated with alveolar macrophages (AMs), were detected in rat lungs following the exposure. Mild to moderate lung pathological changes consisting of increased cellularity, thickening of the alveolar wall, alveolitis, fibrosis, and granuloma formation were detected. Bronchoalveolar lavage (BAL) toxicity parameters such as lactate dehydrogenase activity, number of AMs and polymorphonuclear leukocytes (PMNs), intracellular oxidant generation by phagocytes, and levels of cytokines were significantly ($p < 0.05$) increased

CONTACT Pius Joseph, pcj5@cdc.gov; Tina M. Sager, sst2@cdc.gov, Toxicology and Molecular Biology Branch, National Institute for Occupational Safety and Health, 1000 Frederick Lane, Morgantown, WV 26508, USA.

Disclosure statement

No potential conflict of interest was reported by the author(s). The findings and conclusions in this report are those of the authors and do not necessarily represent the official position of the National Institute for Occupational Safety and Health, Centers for Disease Control and Prevention. The Next Generation Sequence data discussed in this publication have been deposited in NCBI's Gene Expression Omnibus (GEO) and are accessible through GEO Series accession number GSE148869.

in response to exposure to MWCNT-7. Global gene expression profiling identified several significantly differentially expressed genes (fold change >1.5 and FDR *p* value <0.05) in all the MWCNT-7 exposed rats. Bioinformatic analysis of the gene expression data identified significant enrichment of several diseases/biological function categories (for example, cancer, leukocyte migration, inflammatory response, mitosis, and movement of phagocytes) and canonical pathways (for example, kinetochore metaphase signaling pathway, granulocyte and agranulocyte adhesion and diapedesis, acute phase response, and LXR/RXR activation). The alterations in the lung toxicity parameters and gene expression changes exhibited a dose-response to the MWCNT exposure.

Conclusions: Taken together, the data provided insights into the molecular mechanisms underlying the pulmonary toxicity induced by inhalation exposure of rats to MWCNT-7.

Keywords

Multi-walled carbon nanotubes; lung toxicity; molecular mechanisms; inflammation; fibrosis

Introduction

Carbon nanotubes composed of concentric layer(s) of graphene sheet(s) consisting of carbon rings rolled into cylindrical fibers represent a major class among engineered nanomaterials (ENMs). Single-walled carbon nanotubes consist of a single layer of a graphene sheet whereas multiple layers of graphene sheets are present in multi-walled carbon nanotubes (MWCNT). Multi-walled carbon nanotubes, like many other ENMs possess several desirable properties for industrial applications. These include, but are not limited to, their light weight, high aspect ratio and tensile strength, stiffness, and water insolubility which contribute to their enhanced durability. The desirable physicochemical properties of many of the ENMshave facilitated their use in commerce, industry, and medicine (Eatemadi et al. 2014; Stoner et al. 2014). Unfortunately, many of the same desirable properties of ENMs are of concern with respect to their potential for human exposure resulting in adverse health effects. For example, due to their light weight, some of the ENMs can be easily aerosolized, and the air-borne particles may pose a significant threat of exposure by inhalation among workers engaged in the manufacture of products and of consumers who use such products. MWCNT-7, because of its resemblance to asbestos with respect to the thin and needlelike shape and biopersistence, has raised concern about the potential to result in cancer and mesothelioma (Donaldson et al. 2013).

Only limited epidemiological evidence exist for the adverse human health effects associated with exposure to MWCNTs. Many of the studies that investigated the toxicity of MWCNTs have been conducted with a specific form, MWCNT-7, and by employing *in vitro* cell culture and *in vivo* animal models. Compared with the limited evidence for MWCNT-7 exposure to result in cardiovascular (Stapleton et al. 2012) and neurological (Chen et al. 2013) effects, most of the studies have been focused on MWCNT-induced lung toxicity. Exposure of primary cells and immortalized cell lines derived from lungs to MWCNT-7 resulted in cytotoxicity (Siegrist et al. 2014). Similarly, exposure of mouse and rats to MWCNTs following intratracheal administration (Poulsen et al. 2016), pharyngeal aspiration (Porter et al. 2010), and nose-only (Seidel et al. 2021) or whole-body inhalation

(Umeda et al. 2013) also resulted in lung toxicity. The lung toxicity resulting from exposure to MWCNTs was characterized by the induction of inflammation, fibrotic changes, and granuloma formation (Ma-Hock et al. 2009; Porter et al. 2010; Erdely et al. 2013; Umeda et al. 2013; Dong et al. 2015). There have also been a limited number of animal studies that investigated the carcinogenic potential of MWCNT (Sargent et al. 2014; Kasai et al. 2016; Fukushima et al. 2018; Numano et al. 2019; Saleh et al. 2020). In a two-stage, initiator/promoter carcinogenesis model, inhalation exposure of mice to MWCNT-7 resulted in an enhancement in the incidence of methylcholanthrene initiated lung tumor formation (Sargent et al. 2014) which suggested its role as a tumor promoter. Chronic whole-body inhalation exposure of F344 rats to MWCNT-7 at doses of 0.02, 0.2, and 2 μg/m^3 for 104 weeks resulted in dose-dependent increases in the incidence of pre-neoplastic and neoplastic lung lesions suggesting that MWCNT-7 is a complete carcinogen (Kasai et al. 2016) and justified its classification by the International Agency for Research on Cancer (IARC) as a Group 2B human carcinogen (IARC (International Agency for Research on Cancer)) 2017).

Despite the demonstration that MWCNT-7 is toxic to the lungs, the molecular mechanisms underlying its pulmonary toxicity are not fully understood. Determination of the molecular mechanisms underlying the toxicity of MWCNT-7, like any other toxic agent, has implications in assessing the potential risks associated with human exposure to them. Furthermore, understanding the molecular mechanisms of toxicity may be helpful in preventing the toxicity and associated health effects through development of therapeutic agents that target relevant genes and proteins. The use of high content transcriptomics data, in agreement with the US National Research Council's vision of a paradigm shift in toxicology (NRC (National Research Council)) 2007), has enormous potential in determining the mechanisms underlying the target organ toxicity. Simultaneous determination of all genes differentially expressed in a target organ/tissue in response to exposure to a toxic agent, and subsequent bioinformatic analysis of the gene expression data that identifies the significantly enriched pathways and networks have been instrumental in understanding the molecular mechanisms underlying the toxicity of agents including ENMs (Hamadeh et al. 2002; Heinloth et al. 2004; Labib et al. 2016; Nikota et al. 2016; Sager et al. 2020). Therefore, in the current study, rats were exposed to air or increasing doses of MWCNT-7 by whole-body inhalation and the resulting lung toxicity was assessed by histology and BAL parameters of toxicity. Global gene expression profiles in rat lungs were determined by next generation sequence analysis. The transcriptomic data was further analyzed to understand the molecular mechanisms potentially involved in the lung toxicity induced by inhalation exposure of the rats to MWCNT-7. This is the first report investigating the application of global transcriptome analysis to determine the molecular mechanisms of lung toxicity following whole-body inhalation exposure to MWCNT-7 in rats; the species in which the carcinogenicity of MWCNT-7 has been demonstrated (Kasai et al. 2016).

Materials and methods

Generation of MWCNT aerosol and exposure of rats

The MWCNT-7 used in this study was obtained from Mitsui & Company (XNRI MWNT-7, lot #05072001K28, Tokyo, Japan) and has been employed in several studies previously

conducted at our institute (Mercer et al. 2010; Porter et al. 2010; Dong et al. 2015). Details regarding characterization of the MWCNT used in the present study can be found elsewhere (Porter et al. 2010). Stated briefly, the trace metal contamination of the MWCNT-7 sample was 0.78% with sodium and iron accounting for 0.41 and 0.32%, respectively. No other metals were present above 0.02%. The median length of the MWCNT-7 particles was 3.86 μm and the count mean diameter was 49 ± 13.4 nm. Approximately 3-month old, male Fischer 344 rats (CDF strain) were purchased from Charles River Laboratories (Wilmington, MA) and employed in this study. The entire study was conducted in an AAALAC International accredited animal facility (NIOSH, Morgantown, WV, USA) following a protocol approved by the Institutional Animal Care and Use Committee. The rats were allowed to acclimate to the animal facility conditions, at least for 10 days, prior to their use in this study. Throughout the study, the rats were housed in groups of 3 rats/cage and maintained on a 12-hour light-dark cycle in a temperature (68–72 °F) and humidity (30–70%) controlled room. The rats were provided with Teklad rodent diet (Envigo, Indianapolis, IN) and tap water *ad libitum* except when they were exposed to air or the aerosol containing MWCNT as described below.

Generation of MWCNT aerosol and whole-body inhalation exposure of rats were conducted using a previously described automated, computer-controlled system (McKinney et al. 2009, 2013). Aerodynamic particle mass size distribution of the MWCNT aerosol generated for the rat exposure was determined using a micro-orifice uniform deposit impactor (MOUDI Model 110 R, MSP Corporation, Shoreview, MN). Greased foils were used for the MOUDI stages. The mass-median aerodynamic diameter of the air-born MWCNT particles in the exposure chamber was 1.5 μm with a geometric standard deviation (GSD) of 1.67 (Figure 1(A)). A scanning electron microscope (Hitachi S-4800) was used to analyze particle physical morphology by drawing aerosol samples at a flow rate of 1 L/min from the exposure chamber onto 25 mm (0.2 μm pore size) polycarbonate filters (Whatman, Inc., Maidstone, United Kingdom) for approximately 5 seconds. Micrographs showing representative samples of MWCNT particles on the filters are shown in Figure 1(B) and consisted of well dispersed and straight fibers. Groups of rats ($n = 12$) were exposed by whole-body inhalation to the MWCNT aerosol at designated concentrations of 1.25 – 10 μg/m^3, 6 hours/day for 3 consecutive days to result in target cumulative exposure doses (concentration × time) ranging from 22.5 to 180 (mg/m^3)h. Another set of rats ($n = 12$) exposed simultaneously to filtered air, served as controls. Throughout the inhalation exposure, the target levels of temperature (22.2–25.6 °C), humidity (40–60%), and MWCNT concentration in the exposure chamber were continuously monitored and controlled by employing a calibrated mass concentration particle monitor, DataRAM4 (Thermo Fisher Scientific, Waltham, MA, USA) as previously described (McKinney et al. 2009). The health status of the rats was monitored throughout the study and their terminal body weights were recorded.

Euthanasia of rats and collection of biospecimens

Approximately 16-hours following termination of exposure, the rats were euthanized following an intraperitoneal injection of the euthanasia solution containing ≥100 μg sodium pentobarbital/kg body weight (Fort Dodge Animal Health, Fort Dodge, IA, USA).

Blood was collected under anesthesia from the abdominal aorta into Vacutainer tubes containing the anticoagulant, K_2EDTA (Beckton-Dickinson, Franklin Lakes, NJ) and used to determine various hematological parameters. The right lung of the rats was clamped-off and bronchoalveolar lavage (BAL) performed in the left lung (Roberts et al. 2014). The BAL fluid was processed into cellular and acellular fractions and used to determine lung toxicity resulting from inhalation exposure of the rats to air or MWCNT. The apical lobe of the right lung was cut into pieces and stored in RNALater (Invitrogen, Waltham, MA) until isolation of RNA. The cardiac and diaphragmatic lobes of the right lung were inflated with 10% neutral-buffered formalin and fixed in the same solution for histopathological analysis.

Hematology

The hematological parameters analyzed included counts of white blood cells (WBC), red blood cells (RBC), neutrophils (NEUT), lymphocytes (LMPH), monocytes (MONO), eosinophils (EO), basophils (BASO), platelets (PLT), and reticulocytes (RET), red blood cell distribution (RDW), hemoglobin (HGB), hematocrit (HCT), mean corpuscular volume (MCV), mean corpuscular hemoglobin (MCH), platelet distribution width (PDW), mean platelet volume (MPV), and platelet larger cell ratio (P-LCR). These parameters were determined in the unclotted blood samples using an IDEXX Procyte instrument (IDEXX Corporation, Westbrook, ME, USA) following the procedures described in the user guide.

BAL cell counts and lung toxicity determination

The BAL fluid obtained from the rats was centrifuged (570 × g, 15 minutes, 4 °C) to separate the cellular and acellular fractions. The cellular fraction was resuspended in 1 ml PBS and used to determine the number of cells present. Total number of BAL cells [alveolar macrophages (AMs) and polymorphonuclear leukocytes (PMNs)] was determined using a Coulter Multisizer II and Accu Comp software (Coulter Electronics, Hialeah, FL). BAL cells (50,000) were spun onto microscope slides using a Cytospin 3 centrifuge (Shandon Life Sciences International, Cheshire, UK) and stained with a Leukostat stain (Fisher Scientific, Pittsburgh, PA) to differentiate AM from PMNs. Approximately two hundred cells were counted per rat, and PMN percentages were multiplied back across the total cell count to obtain total AM and PMN numbers. The cytospin slides were also examined under a light microscope for the presence of MWCNT-7 particles. The acellular fraction of the BALF was used to determine LDH activity, a marker for increased membrane permeability due to damage or death of lung inflammatory and/or epithelial cells, using a Cobas c111analyzer (Roche Diagnostic Systems, Mont Clair, NJ, USA).

Reactive oxidant generation by lung phagocytes

Intracellular levels of reactive oxidants generated by the lung phagocytes was estimated by a luminol-dependent chemiluminescence assay using a Berthold LB 953 luminometer (Wildbad, Germany) as described previously (Roberts et al. 2014). Stated briefly, phorbol 12-myristate 13-acetate (PMA), a soluble stimulant of total BAL phagocytes (AM and PMNs) or nonopsonized, insoluble zymosan, a stimulant of AM only, were used to determine the contribution of both AM and PMN to the overall production of intracellular ROS by the lung phagocytes. The chemiluminescence assay was performed in the presence or absence of the stimulants. The light generation was recorded for 15 minutes at 37 °C,

and the integral of counts per minute (CPM) per 10^6 cells versus time was determined. The difference in the CPM of the stimulated and corresponding unstimulated cells was calculated. The calculated value was normalized to the total number of BAL cells for PMA-stimulated chemiluminescence and total number of AM in the BAL for zymosan-stimulated chemiluminescence.

Cytokine analysis

The acellular first fraction of BALF was used to determine cytokines, released by the inflammatory and/or epithelial cells in response to pulmonary exposure to MWCNT and play critical role in the influx of additional inflammatory cells resulting in lung inflammation and/or injury. BALF levels of cytokines, viz: interleukin 1β (IL-1β), interleukin 10 (IL-10), interleukin 13 (IL-13), interleukin 16 (IL-16), interleukin 18 (IL-18), tumor necrosis factor-α (TNF-α), monocyte chemotactic protein-1 (MCP-1), and macrophage inflammatory protein-2 (MIP-2) were determined by employing the rat magnetic panel of a Milliplex Map Kit (Millipore, Inc. Billerica, MA) following the instructions provided by the vendor.

Lung histopathology

The diaphragmatic and cardiac lobes of the left lung, fixed in formaldehyde, were embedded in paraffin, sectioned at a thickness of 5 μm, stained with hematoxylin and eosin or Mason's trichrome stain and examined for histological changes by a pathologist. The lung histological changes were scored as none (normal histology), minimal (<10% thickening of the alveolar wall in focal areas with little or no inflammatory cells occupying <10% of the lung parenchyma and no granuloma per section), mild (10–25% thickening of the alveolar walls in focal areas with a few inflammatory cells occupying 10–20% of the lung parenchyma and 1–5 granuloma per section), or moderate (approximately 2-fold thickening of the alveolar walls in focal areas with plenty of inflammatory cells occupying 20–40% of the lung parenchyma and more than 5 granuloma per section).

RNA isolation and determination of global gene expression profile in lungs

Total RNA free of contaminating DNA and proteins was isolated from a piece of the lung tissue stored in RNALater using miRNEasy Mini Kit (Qiagen, Inc. Valencia, CA) following the procedure, including the on-column DNase digestion, provided by the manufacturer. The RNA samples were quantified by UV-Vis spectrophotometry and their integrity and purity were determined using an Agilent 2100 Bioanalyzer and RNA 6000 Nano Kit (Agilent Technologies, Palo Alto, CA). All the RNA samples used in the gene expression studies exhibited an RNA Integrity Number (RIN) ≥8.0.

The Illumina TruSeq® mRNA Library Prep Kit (Illumina, Inc. San Diego, CA, USA) was used to create next generation sequencing (NGS) libraries following the procedures described in our previous publication (Joseph et al. 2021). Briefly, RNA (1 mg/sample) was fragmented (68 °C for 5 minutes) and purified following depletion of ribosomal RNA (rRNA). The RNA fragments were reverse transcribed into first strand cDNA using reverse transcriptase and random primers. For proper adaptor ligation, while synthesizing the double stranded cDNA, dUTP was incorporated in place of dTTP followed by the

addition of a single 'A' nucleotide to the 3 prime ends. Indexing adapters provided in the library preparation kit were ligated to the ends of the ds cDNA. The adaptor-ligated cDNA fragments were PCR amplified (12 cycles) using a Veriti™ 96 Well Thermal Cycler (Applied Biosystems, Foster City, CA, USA) and quantified using a dsDNA HS Assay Kit (Invitrogen by ThermoFisher Scientific, Waltham, MA, USA) and Qubit 3.0 Fluorometer (Invitrogen by ThermoFisher Scientific, Waltham, MA, USA). Average fragment size and fragment distribution of the cDNA library samples were then assessed using an Agilent 2100 Bioanalyzer with High Sensitivity DNA Reagents (Agilent Technologies, Santa Clara, CA).

Individual sample libraries were sequenced (Genome Sequencing Laboratory, The Centers for Disease Control and Prevention, Atlanta, GA) for 2 × 75 base pair, paired-end sequencing using the Illumina Hiseq 2500 machine (Illumina, San Diego, CA, USA) in rapid run mode using HiSeq Rapid Cluster Kit v2 and HiSeq Rapid SBS Kit v2 (Illumina, San Diego, CA, USA). After demultiplexing the library sequences, the quality of each sample library was assessed with respect to the number of reads per sample, mean quality score, and FASTQC parameters (Andrews 2010). Reads were then processed using Trimmomatic/0.35 with the options PE, ILLUMINACLIP:TruSeq2-PE.fa:2:30:10 LEADING:3 TRAILING:3 SLIDINGWINDOW:4:15 MINLEN:85 to remove any remaining adapter sequence, low quality reads, low quality read ends, and sequences shorter than 85 bases in length (Bolger et al. 2014). Sequence quality was then reevaluated via FASTQC. All sequences that passed the trimming and quality control with both reads in a pair present were aligned to the *Rattus norvegicus* Rnor 6.0 genome from NCBI downloaded July 31st, 2015 using HiSat2/2.1.0 (Kim et al. 2015). Raw gene counts were assigned using Samtools/1.9 (Li et al. 2009), Python/2.7.3 and HTSeq/0.6.1. Rnr1 (Ribosomal 45S Cluster 1) and Rnr2 (Ribosomal 45S Cluster 2) displayed extremely high counts and were manually removed before further analysis. Using edgeR, raw counts were converted to counts per million (CPM), log-CPM, and normalized using the trimmed mean of M-values (TMM) method. Finally, differentially expressed genes were calculated using limma (Law et al. 2016; R Core Team 2018). Significantly differentially expressed genes (SDEGs) were those genes with an absolute fold change greater than 1.5-fold and an adjusted p-value less than 0.05.

Bioinformatic analysis of gene expression data

The SDEGs identified by NGS analysis were used as input for subsequent bioinformatic analysis using the Ingenuity Pathway Analysis program (IPA, Ingenuity Systems, Redwood City, CA). IPA software is designed to map the biological relationship of the uploaded genes and classify them into categories according to published literature in the database. Non-lung related IPA categories that are not relevant to the present study were filtered out. The bioinformatic analysis of the gene expression data by employing the IPA program facilitated the extraction of toxicologically meaningful information from the list of the large number of SDEGs detected in response to inhalation exposure of the rats to MWCNT-7 aerosol particles. Fisher's exact test was conducted to calculate p-value to determine the significance of a particular biological function or canonical pathway enriched by MWCNT-7 exposure in the lungs ($p < 0.05$ was considered statistically significant).

Statistical analysis of the data

Data between the MWCNT-7 exposed and the control group of rats, excepting the NGS data, were compared using the one-way analysis of variance (ANOVA) test. *Post hoc* comparisons were made with Fisher's least significant difference (LSD) test. Data analyses were performed using JMP version 13.2 for Windows. The level of statistical significance was set at $p < 0.05$.

Results

Clinical signs of toxicity

Statistically nonsignificant reductions in the terminal body-weights of rats exposed to MWCNT-7 at the higher cumulative doses of 90 and 180 (mg/m^3)h MWCNT-7, compared with the respective controls, were observed (data not presented). There were no clinical signs of toxicity in any of the rats in response to their exposure to MWCNT-7.

Lung deposition of MWCNT-7

Inhalation exposure of rats to the aerosol containing MWCNT-7 resulted in deposition of the inhaled MWCNT-7 particles in the lungs, including in the deep alveolar regions (Figure 2(B)) where the particles were engulfed by the alveolar macrophages (Figure 2(D)). The animal exposures to MWCNT-7 at cumulative doses of 22.5–180 (mg/m^3)h resulted in an estimated alveolar deposited dose ranging from 8.2 to 69 mg based on the multi-path particle dosimetry (MPPD) model (Anjilvel and Asgharian 1995). The MPPD version 3.04 with semi-symmetric settings for rats with a breathing frequency of 102 breathing/minute and a tidal volume of 2.1 ml was used. The MMAD and GSD from the MUODI data were used in the MPPD mode to calculate the human equivalence of the dose exposed in the rats. The exposure dose can be scaled to a human equivalent dose by using known alveolar surface area values of 70 m^2 and 0.4 m^2, respectively, for human and rat lungs (Butler 1976; Ohashi et al. 1994). By using these values, the equivalent human alveolar lung burden resulting from the MWCNT-7 exposures was estimated and found to range from 1,435 to 12,094 mg. Assuming that the deposition efficiency of the particles is 14% in the human pulmonary region and a human minute ventilation of 15 L/min, the rat exposures conducted in this study would be equivalent to an average worker's exposure over a single 40-hour work week at a MWCNT-7 aerosol concentration ranging from 0.34 to 2.84 mg/m^3. The NIOSH recommended exposure limit (REL) of elemental carbon (EC), an indicator of occupational exposure to CNM, is 1 $\mu g/m^3$ for an 8-hour time-weighted average (NIOSH (National Institute for Occupational Safety and Health)) 2013). The amount the EC present in the inhalable size fraction of the aerosol samples collected from facilities manufacturing CNMs was 6.22 $\mu g/m^3$ (Dahm et al. 2018) and 3.51 – 17.14 $\mu g/m^3$ (Fatkhutdinova et al. 2016). The EC mass in the personal breathing zone samples collected from some of the U.S. facilities engaged in the manufacture and handling of CNMs was 7.54 $\mu g/m^3$ (Dahm et al. 2012) and 10.6 $\mu g/m^3$ (Erdely et al. 2013).

Lung histology

Moderate histological changes were detected in the lungs of the rats exposed to the highest cumulative dose of 180 (mg/m^3)h MWCNT-7 (Figure 3(D)). The most prominent lesion in this group was intra-alveolar granulomas consisting of round-shaped accumulation of inflammatory mononuclear cells. Typically, the granulomas were <100 microns in diameter and often associated with particles/filaments that occupied the wall and protruded into the alveolar lumina. The granulomatous lesions were prominent and were seen in all (12/12) the exposed animals. Trichrome staining showed that these early granulomas contained a slightly elevated number of collagen fibers, i.e., early fibrosis (data not presented). In addition to the granulomatous lesions, there were areas of early alveolitis with increased cellularity and increased alveolar wall thickness. Quite often these areas of alveolitis, like the granulomas, were associated with black MWCNT-7 pigmented granules and filaments, seen both inside the alveolar walls and in the alveolar and bronchiolar lumina. Also, airway epithelial hyperplasia characterized by epithelial folding and crowding of the pseudostratified columnar epithelium and sometimes excessive mucous cell numbers (mucous metaplasia) was seen in all the lung sections.

In the 90 (mg/m^3)h cumulative dose group, the same histological changes detected in the 180 (mg/m^3)h group, were detected (Figure 3(C)). However, changes were markedly less intense, especially at the level of the granulomatous lesions that were fewer in number and smaller in size compared with the 180 (mg/m^3)h group. Nevertheless, the presence of granulomatous inflammatory lesions (granuloma precursors because of their small size) were seen in most cases (9/12). Trichrome stain also showed very early fibrosis associated with the inflammatory and granulomatous lesions (but clearly less and more difficult to detect than in the previous group). Airway epithelial hyperplasia was less prominent and seen in only 7/12 MWCNT-7 exposed rats.

The 45 (mg/m^3)h cumulative dose group of rats had minimal histological changes, i.e., small areas of focal alveolitis and airway epithelial hyperplasia in less than 25% of the MWCNT-7 exposed rats (Figure 3(B)). No granulomatous lesions were detected in this group of rats. Intra-alveolar macrophages were elevated in all exposed rats but at a much less prominent level compared with the higher dose groups of rats. Small focal areas of alveolitis with slightly increased cellularity and alveolar thickness was seen sporadically in some of the control, air exposed rats which is considered as background lesions (Figure 3(A)). The lung histology of the rats exposed to the lowest, 22.5 (mg/m^3)h cumulative dose of MWCNT-7, was similar to that of the control, air exposed rats (micrograph not presented).

BAL parameters of lung toxicity

None of the BAL parameters of toxicity analyzed in the rats, viz. LDH, total BAL cells, AM, and PMN, exhibited any difference in the rats exposed to the lowest cumulative dose of 22.5 (mg/m^3)h compared with the corresponding control group (Figure 4(A–D)). However, all groups of the rats exposed to MWCNT-7 at cumulative doses of 45 (mg/m^3)h and above, exhibited alterations in all these parameters. These alterations were statistically significant only in the higher dose groups of 90 and 180 (mg/m^3)h in the case of LDH activity and the PMN count (Figure 4(A,D)). On the other hand, the numbers of total BAL cells and AM

were significantly higher ($p < 0.05$) in the rats exposed to MWCNT-7 at cumulative doses of 45, 90, and 180 (mg/m^3)h, compared with the corresponding controls (Figure 4(B,C)). The highest increase among the BAL parameters of lung toxicity analyzed was detected in the case of the PMN number which exhibited a 111.32-fold increase in the rats exposed to 180 (mg/m^3)h MWCNT-7, compared with the control rats. Additionally, the increases in the BAL parameters of toxicity were dependent on the dose of the MWCNT-7 inhaled in majority of the cases.

Lung oxidant generation

Both the zymosan- and PMA-stimulated chemiluminescence, in all groups of the rats exposed to MWCNT-7 aerosol, compared with the respective controls, exhibited dose-dependent increases (Figure 5(A,B)). Furthermore, these increases were statistically significant ($p < 0.05$) in the rats exposed to MWCNT-7 at cumulative doses of 45, 90, and 180 (mg/m^3)h.

Lung cytokine analysis

All eight cytokines analyzed in the rats showed increased BALF levels, compared with the respective controls (Figure 6). Furthermore, the increases in the cytokines were dependent on the dose of MWCNT-7 inhaled by the rats. In the case of IL-13, the increases in all 4 dose groups were statistically significant ($p < 0.05$) compared with the respective controls (Figure 6) whereas for IL-1β, IL-10, and IL-16, statistically significant increases were detected in the higher three dose groups (Figure 6). In the case of IL-18, TNF-α, MCP-1, and MIP-2, statistically significant increases were detected in the rats that belonged to the cumulative exposure groups of 90 and 180 (mg/m^3)h MWCNT-7 (Figure 6).

Hematology

Slight but statistically significant increases in hematological parameters such as WBC, reticulocytes, MCV, and MCH were detected in the rats exposed to the highest cumulative dose of 180 (mg/m^3)h MWCNT-7 (data not presented).

Lung gene expression profile

Several SDEGs were identified in the lungs of the MWCNT-7 exposed rats (Figure 7). The total number of SDEGs detected in the lungs were 405, 395, 612, and 980 in the rats that were exposed to MWCNT-7 at the cumulative doses of 22.5, 45, 90, and 180 (mg/m^3)h, respectively. Among the SDEGs identified, at least 80% of the genes were overexpressed in each of the four dose groups of the rats. Furthermore, 214 SDEGs were common to all four dose groups while the number of unique SDEGs were 49, 56, 73, and 461, respectively in the 22.5, 45, 90, and 180 (mg/m^3)h groups (data not presented). Similar to the number of the SDEGs, the fold changes in expressions of many of the SDEGs were also dependent on the MWCNT-7 dose to which the rats were exposed (Table 1).

Bioinformatic analysis of the SDEGs identified the IPA biological functions and canonical pathways that were significantly enriched in the rat lungs in response to MWCNT-7 exposure. Lung cancer, leukocyte migration, inflammatory response, mitosis, cell movement of phagocytes, recruitment of leukocytes, inflammation of airway, accumulation of

leukocytes, recruitment of phagocytes, and activation of macrophages were among the top ranking, enriched IPA biological functions (Figure 8(A)). The IPA canonical pathways that were significantly enriched and ranked high were kinetochore metaphase signaling pathway, granulocyte adhesion and diapedesis, agranulocyte adhesion and diapedesis, acute phase response signaling, LXR/RXR activation, complement system, TREM1 signaling, phagosome formation, cell cycle control of chromosomal replication, and communication between innate and adaptive immune cells (Figure 8(B)).

Discussion

Human exposure to MWCNT-7 is concerning because of its potential to result in serious adverse health effects. The potential for MWCNT-7 to result in adverse health effects is primarily because of its small, nanoscale size, its rigidity and durability as well as the needlelike shape, similar to those of asbestos and other pathogenic fibers, and its ability for biopersistence (Donaldson et al. 2013). While exposure to carbon-based nanomaterials taking place among workers has been reported in the US (Beard et al. 2018) and elsewhere (Lee et al. 2015), most of the evidence for potential adverse human health effects of MWCNT-7 is derived from the results of animal studies. Primarily because of their light weight, MWCNT-7 particles can be easily aerosolized, thus posing the highest risk for exposure by inhalation potentially resulting in pulmonary and systemic toxicity. Lung toxicity in mice and rats following pulmonary exposure to MWCNT by pharyngeal aspiration, intratracheal instillation, or inhalation has been investigated in the past. In an earlier dose-response and time-course study, Porter et al. (2010) administered MWCNT-7 in mice by pharyngeal aspiration at doses of 0, 10, 20, 40, and 80 mg and the resulting lung toxicity was determined at post-exposure time intervals of 1, 7, 28, and 56 days. Based on the results of BAL parameters of toxicity and lung histology, the authors concluded that MWCNT-7 exposure resulted in dose-dependent and persistent lung inflammation, damage, and granuloma formation. Intratracheal administration of MWCNT particles also resulted in inflammation, fibrosis, and granuloma formation in mice (Poulsen et al. 2016) and rats (Muller et al. 2005). Lung toxicity has also been investigated, following inhalation exposure to aerosolized MWCNT particles in mice (Mercer et al. 2013; Porter et al. 2013) and rats (Ma-Hock et al. 2009; Delorme et al. 2012; Umeda et al. 2013; Kasai et al. 2015; Gate et al. 2019). Results obtained from these studies also demonstrated that inhalation exposure to MWCNT particles resulted in persistent inflammation, injury, fibrosis, and granuloma formation in the rodent lungs. The MWCNT-7 particles deposited in the rodent lungs are also capable of penetrating the alveolar wall (Mercer et al. 2010) and reaching the subpleural tissue (Ryman-Rasmussen et al. 2009) to result in mesothelioma as reported following intraperitoneal and intrascrotal administration of MWCNT in mice (Takagi et al. 2008) and rats (Sakamoto et al. 2009), respectively.

In the current study, rats were exposed by whole body inhalation to an aerosol containing increasing concentrations of MWCNT-7 which, as expected from the results of several previously conducted *in vivo* animal studies (Muller et al. 2005; Ma-Hock et al. 2009; Porter et al. 2010 and 2013; Delorme et al. 2012; Umeda et al. 2013; Kasai et al. 2015; Poulsen et al. 2016), resulted in lung toxicity. Granuloma formation, a feature characteristic to the lung damage associated with pulmonary deposition of persistent and toxic fibrous particles,

for example asbestos (Donaldson et al. 2006), was detected in the lungs of the MWCNT-7 exposed rats, especially those exposed to the highest cumulative dose of 180 (mg/m^3)h (Figure 3(A–D)) which was equivalent to ~69 mg deposited dose by MPPD calculation. The LDH activity, considered to be an indicator of cytotoxicity including that induced by exposure to inhalable, lung toxic particles (Sager et al. 2020; Joseph et al. 2021), was increased in the rat lungs that were exposed to MWCNT-7 at cumulative doses of 45 (mg/m^3)h and higher (Figure 4(A)). Similarly, the BAL cell counts, determined in the MWCNT exposed rats, were significantly ($p < 0.05$) increased except for the group that was exposed to the lowest cumulative dose of 22.5 (mg/m^3)h or approximately 8.2 μg deposited dose (Figure 4(B–D)). This suggested the induction of inflammation in the lungs of the MWCNT exposed rats. Generation of reactive oxidants, found to be associated with the pathology of respirable particles (Sager et al. 2020; Joseph et al. 2021), was also significantly higher ($p < 0.05$) in the rat lungs which were exposed to MWCNT-7 at cumulative doses 45 (mg/m^3)h and higher (Figure 5(A,B)). Determination of the BALF levels of eight cytokines and chemokines that are known to be involved in the inflammatory response to exposure to toxic particles (Laskin and Laskin 2001) revealed significant elevations in the MWCNT-7 exposed rat lungs, compared to those detected in the air exposed, control lungs (Figures 6). All the parameters that were employed to determine the lung response to MWCNT-7 exposure exhibited alterations, especially in the lungs exposed to the higher cumulative doses. These results, therefore, suggested the induction of lung toxicity in the rats by their whole-body inhalation exposure to MWCNT-7 particles under the conditions employed in the current study. Furthermore, the alterations in the toxicity parameters determined were dependent on the cumulative dose of MWCNT-7 to which the rats were exposed.

It has been well established that the transcriptome is a sensitive target that responds to exposure to toxic agent(s) and, therefore, transcriptome profiling has been employed to detect target organ toxicity (Joseph 2017). Similarly, determination of the global gene expression profile in the target organ(s) of toxicity and further bioinformatic analysis of the differentially expressed genes have been employed to understand the molecular mechanism(s) involved in the toxicity (Hamadeh et al. 2002; Labib et al. 2016; Sager et al. 2020; Joseph et al. 2021). Currently, determination of the global gene expression profile in the rat lungs identified changes in the expression levels of several genes in response to exposure to MWCNT-7. The number of the SDEGs detected in the rat lungs (Figure 7), like the alterations in the toxicity parameters detected, exhibited a dose-response to the cumulative dose of MWCNT-7 exposed. A similar quantitative relationship was also noticed between the alterations in the various lung toxicity parameters and the enrichment in the IPA biological and canonical pathway categories (Figure 8(A,B) suggesting that the gene expression changes detected in the rat lungs, in response to their exposure to MWCNT-7, were mechanistically relevant to the lung toxicity induced by MWCNT-7.

Inhaled toxic particles such as MWCNT-7, upon deposition in the lungs, are engulfed by phagocytes, mostly AMs, for their detoxification and elimination thus preventing their participation in the induction of lung damage. In agreement with the results of previous studies (Mercer et al. 2010, 2013; Kasai et al. 2015), MWCNT-7 particles deposited in the rat lungs were found both associated with the AMs and free in the alveoli (Figure 2). The significant increase in the number of the AMs detected in the MWCNT-7 exposed rat lungs

(Figure 4(C)) may be considered an adaptive response due to the increased demand for the AMs to facilitate the phagocytosis and thus detoxification of the toxic MWCNT-7 particles. This view is further supported by the significant and MWCNT-7 dose-dependent enrichment in the IPA categories recruitment of phagocytes, activation of macrophages, and phagosome formation (Figure 8(A,B) as well as differential expressions of the genes involved in those categories (Table 1). The interaction between the toxic particles deposited in the lungs and the AMs may result in macrophage activation and the release of various signaling molecules. Activation of AMs, in response to inhalation exposure to MWCNT-7, was supported by the dose-dependent increase in the transcript, *RETNLA1,* a marker for macrophage activation (Nair et al. 2009), in the MWCNT-7-exposed rat lungs (Table 1). Cytokines/chemokines represent one major class of the signaling molecules released by the activated AMs (Becker et al. 1991). The transcripts for several cytokines/chemokines viz. *CCl2, CCl7, CCl9, CCL22, CXCl2, CXCl3, CXCl6,* and *CXCL10* were significantly overexpressed in the MWCNT-7 exposed rat lungs (Table 1). Similarly, the BAL protein levels of all eight cytokines/chemokines analyzed were significantly elevated in the MWCNT-7 exposed rats (Figure 6). The cytokines/chemokines released by the macrophages are involved in the recruitment of additional macrophages to the lungs, activation of the macrophages, and phagocytosis of toxic particles by the AMs and, therefore, are important determinants deciding the fate of the particles with respect to their potential to induce lung toxicity. MWCNT-7 particles, mainly because of their insolubility, were poorly eliminated from the alveoli which resulted in their accumulation, persistence, and the ensuing toxicity as supported by the MWCNT-7 dose-dependent histological changes (Figure 3) and increases in the LDH activity (Figure 4(A)) detected in the lungs.

Induction of inflammation has been identified as a major mechanism involved in the lung toxicity and the potential for health effects resulting from exposure to MWCNT (Porter et al. 2010 and 2013; Poulsen et al. 2016; Dong and Ma 2016a). In the present study, inhalation exposure of rats to MWCNT-7 resulted in significant and dose-dependent lung inflammation as evidenced by increases in the BAL levels of PMNs (Figure 4(D)) and all eight cytokines/chemokines analyzed (Figure 6). One of the first responses to pulmonary exposure to toxic foreign molecules is the recruitment of phagocytes, primarily PMNs, from blood to the lungs. This takes place mainly in response to the pro-inflammatory signaling molecules released in response to the interaction of the inhaled toxic particles with the AMs and/or the lung epithelium. The recruitment of PMNs from the circulatory system to the lungs is a complex, multistep process which involves tethering, activation, adhesion to the endothelium, rolling, and transmembrane release (Mizgerd 2002). The entire process is controlled by many signaling molecules including the cytokines/chemokines that belong to the CC and CXC families (Mizgerd 2002). The transcripts for several of these cytokines/chemokines, similar to those reported in mice exposed to the same MWCNT-7 (Snyder-Talkington et al. 2013; Dymacek et al. 2018) that was employed in our rat study, were overexpressed in the lungs of the MWCNT-7 exposed rats (Table 1). The overexpression of the transcripts for pro-inflammatory cytokines/chemokines in the lungs (Table 1), pulmonary infiltration of the PMNs (Figure 4(D)), and the lung injury (Figures 3 and 4(A)) all exhibited a response to the cumulative MWCNT-7 dose to which the rats were exposed suggesting a possible relationship among overexpression of cytokines/chemokines, pulmonary infiltration

of PMNs, and the lung injury detected in the MWCNT-7 exposed rats. These results, in agreement with the results of previous studies (Porter et al. 2010 and 2013; Poulsen et al. 2016; Dong and Ma 2016a), furthermore supported the important role inflammation played in the MWCNT-induced lung injury in the rats.

Results of the bioinformatic analysis of the SDEGs further supported the involvement of inflammation in MWCNT-7-induced lung toxicity as well as provided information about the potential molecular mechanisms underlying the toxicity. This included the enrichment of inflammation-related IPA biological functions such as inflammatory response and inflammation of airways (Figure 8(A)) and canonical pathways such as acute phase response signaling, LXR/RXR activation, complement system, and TREM1 signaling (Figure 8(B)) as well as the significant increases in the expression levels of several genes belonging to those categories in the MWCNT-7 exposed rat lungs (Table 1). The acute phase response is a rapid inflammatory response to defend tissues/organs against invading microorganisms (Perez 2019) and injury resulting from exposure to toxic agents (Saber et al. 2014). However, enhanced activation of the acute phase response and excessive release and accumulation of acute phase response signaling molecules may result in tissue damage and toxicity. Serum amyloid is a marker for acute phase response (Sack 2018) and a significant overexpression of the *Serum amyloid A like 1* (*Saal1)* transcript was detected in the MWCNT-7 exposed rat lungs (Table 1). Similarly, the transcript for another gene, *Orosomucoid 1 (ORM1),* involved in the acute phase response and inflammation (Alfadda et al. 2012; Ligresti et al. 2012) was highly overexpressed in the MWCNT-7 exposed rat lungs (Table 1), which further supported the involvement of acute phase response in the lung inflammation and toxicity induced by MWCNT-7, similar to that resulting from exposure to other particles that are toxic to the lungs (Sager et al. 2020; Joseph et al. 2021). Like the acute phase response, activation of the complement system is another important mechanism involved in immunity and inflammatory response to tissue injury by toxic particles (Pandya and Wilkes 2014). Complement proteins, regulators of the complement system, are synthesized by lung epithelial cells (Strunk et al. 1988; Varsano et al. 2000) and fibroblasts (Volanakis 1995) in response to the release of pro-inflammatory cytokines (Huber-Lang et al. 2002). The complement proteins, in turn, may function as chemoattractants facilitating the infiltration of PMNs into the lungs to result in the induction of inflammation such as that was currently detected in the MWCNT-7 exposed rat lungs (Figures 4 and 6). The transcripts for many of the genes involved in complement response, viz. *Complement C1s (C1S), Complement 3 (C3), Complement 6 (C6), Complement factor B (CFB), Complement C1q A chain (C1QA), Complement C1q B chain (C1QB), Complement C1q C chain (C1QC), Integrin subunit alpha M (ITGAM),* and *Integrin subunit alpha X (ITGAX),* and *Integrin subunit beta 8 (ITGβ8)* were overexpressed in the rat lungs and their overexpression was dependent on the cumulative MWCNT-7 dose to which the rats were exposed (Table 1). Taken together, these findings suggested the activation of the complement system and its potential involvement in the MWCNT-7-induced lung inflammation and injury detected in the rats. Triggering receptor expressed on myeloid cells 1 (TREM1) is a receptor that belongs to the immunoglobulin family of cell surface receptors. The association between activated TREM1 and its partners, the toll-like receptors (TLR), facilitates the release of cytokines such as MCP-1, MIP-2, and TNF-α (Bleharski et al. 2003; Ornatowska et al. 2007) resulting in

a pro-inflammatory response. The significant overexpression of the transcripts for *TREM1* and several *TLRs* (Table 1) as well as the elevated BALF levels of cytokines (MCP-1, MIP-2, and TNF-α) (Figure 6F-H) detected in the lungs are suggestive of the potential involvement of the TREM1 signaling pathway in the induction of lung inflammation and injury that resulted from inhalation exposure of the rats to MWCNT-7.

Generation of reactive oxidants and the resulting oxidative stress is a major mechanism involved in the toxicity and pathology associated with exposure to particles of human health concern. The toxic particles may possess ROS on their surface which, upon interaction with the biological system, may result in oxidative stress and injury (Castranova 1994). Metals such as iron present as impurities with particles may also generate ROS through Fenton reaction to result in oxidative stress (Fubini et al. 1991). The third mechanism involved in the induction of particle-induced oxidative stress is due to the interaction of the particles with the phagocytes and the resulting oxidative burst and release of the particles and reactive oxidants (Donaldson et al. 2013). It has been reported that MWCNT-7 particles do not directly generate ROS (Fenoglio et al. 2006). Similarly, the MWCNT-7 sample that was currently employed to generate the aerosol for rat inhalation exposure does not contain iron that is either bioavailable or redox sensitive (Porter et al. 2010) thus ruling out the involvement of Fenton reaction as a possible mechanism responsible for the ROS generation detected in the rat lungs. The detection of intracellular levels of reactive oxidants in the rat lungs, in response to their inhalation exposure to MWCNT-7 aerosol (Figure 5) may, therefore, suggest that the oxidant generation detected was facilitated indirectly by the interaction of the particles with the lung phagocytes.

The gene expression data and findings of the bioinformatic analysis also supported the MWCNT-7-induced oxidative stress in the rat lungs. The nuclear factor erythroid-2 related factor 2 (NRF2) is a redox sensitive transcription factor that regulates the expression of key genes involved in protecting the biological system through detoxification of toxic reactive oxidants (Kensler et al. 2007). The MWCNT-7-induced oxidative stress, pulmonary inflammation, and fibrosis were significantly higher in the NRF2 knock-out mouse, compared with the wild type mouse (Dong and Ma 2016a), suggesting a protective role for NRF2 in the deleterious effects associated with MWCNT-7 exposure. Genes that are members of the canonical pathway, NRF2-mediated oxidative stress, were significantly overexpressed in the lungs of the MWCNT-7 exposed rats. For example, *Superoxide dismutase 2 (SOD2)* – an NRF2-regulated gene that was significantly overexpressed in the lungs of the MWCNT-7 exposed rats (Table 1) is primarily responsible for the generation of hydrogen peroxide, a toxic ROS, by dismutation of the superoxide anion. The *NADPH oxidase organizer 1* (*NOXO1)* gene involved in the generation of toxic superoxide anion (Katsuyama et al. 2012) was also highly overexpressed in the MWCNT-7 exposed rat lungs (Table 1). Other genes involved in oxidative stress response such as *Lactoperoxidase (LPO)* (Sharma et al. 2013), *Hemeoxygenase 1 (HMOX1)* (Nakashima et al. 2018), and *Lipocalin 2 (LCN2)* (Roudkenar et al. 2007), also exhibited a significant and dose-dependent overexpression in the MWCNT-7 exposed rat lungs (Table 1). The absence of efficient detoxification of the ROS generated may facilitate their accumulation in the lungs resulting in oxidative stress and injury including excessive inflammation and fibrosis, as previously

reported in the case of NRF2 knock out mouse, in response to MWCNT-7 exposure (Dong and Ma 2016a).

Physical characteristics of MWCNT-7 such as high aspect ratio, fibrous, needlelike shape, rigidity, and insolubility contributing to biopersistence are concerning especially with respect to their potential to result in fibrosis resembling that of a foreign substance-induced fibrosis (Donaldson et al. 2006; Dong et al. 2015). The detection of collagen fibers by trichrome staining, an indicator of fibrosis, in the MWCNT-7 exposed rat lungs (data not presented) was mild in nature most likely due to the short duration of the current study. Nevertheless, the results of our study, in agreement with those of several *in vivo* studies (Porter et al. 2010; Dong et al. 2015; Kasai et al. 2015, 2016), confirmed the fibrogenic potential of MWCNT-7.

Many of the SDEGs identified in the MWCNT-7 exposed rat lungs were known for their role in tissue fibrosis. The *Serpine family E member 1* (*SERPINE1)* gene plays a pivotal role in lung diseases through its involvement in chronic inflammation (Tiwari et al. 2016), tissue remodeling (Chen et al. 2021), and fibrosis (Ghosh and Vaughan 2012). Furthermore, SERPINE1 gene polymorphism is a risk factor for respiratory diseases (Chen et al. 2021) and inhibitors of SERPINE1 protein have therapeutic application in treating upper respiratory diseases (Huang et al. 2012). Considering the role of SERPINE1 gene in respiratory diseases, the significant overexpression of its transcript currently detected in the lungs of the rats (Table 1) should be of functional significance to the MWCNT-7-induced lung fibrosis. Other genes whose expressions were significantly higher in the MWCNT-7 exposed rat lungs, compared with the controls, and potentially involved in the MWCNT-7-induced fibrosis were *Secreted phosphoprotein 1 (SPP1), TIMP metallopeptidase inhibitor 1 (TIMP1), Chitinase, acidic (CHIA), Adenosine A1 receptor (ADORA1), Pentraxin 3 (PTX3),* and *Matrix metallopeptidase 12 (MMP12).* Osteopontin, the protein product of the SPP1 gene, through activation of the TGF-β signaling pathway, facilitates the activation and differentiation of fibroblasts to myofibroblasts – a critical step involved in fibrosis (Dong and Ma 2017). A similar role for TIMP1 in the MWCNT-7-induced lung fibrosis through activation and proliferation of fibroblasts has been identified (Dong and Ma 2016b). Extracellular matrix (ECM) formation, a critical event in fibrosis, is a complex process that involves the synthesis and degradation of ECM proteins, most notably collagen. The significant overexpression of *ADORA1, CHIA, MMP12,* and *PTX3* in the MWCNT-7-exposed rat lungs, their established role in the maintenance of the ECM (Churg and Wright 2005; Cronstein 2011; Lee et al. 2012; Pilling et al. 2015), and the increase in collagen detected in the lungs should be considered as evidence for their potential involvement in the MWCNT-7-induced lung fibrosis in the rats.

The International Agency for Research on Cancer (IARC), based on the results of animal studies, has classified one form of the MWCNT, MWCNT-7, the same material used in this study, as a Group 2B human carcinogen (IARC (International Agency for Research on Cancer)) 2017). Whereas MWCNT-7 was identified as a tumor promoter in a mouse model (Sargent et al. 2014), prolonged inhalation exposure to MWCNT-7 alone resulted in significant increases in pre-neoplastic and neoplastic lesions in the rat lungs suggesting that MWCNT-7 is a complete carcinogen (Kasai et al. 2016). Despite the identification

of MWCNT-7 as a carcinogen, the mechanisms underlying its carcinogenicity are yet to be fully determined. The absence of positive results in the Ames test (Ema et al. 2012) suggested that the carcinogenicity of MWCNT-7 may not be due to its role as a direct mutagen. On the other hand, changes in chromosome number were detected in cultured cells in response to exposure to MWCNT-7 (Asakura et al. 2010; Siegrist et al. 2014) attributing induction of aneuploidy as a potential mechanism involved in the MWCNT-7-induced carcinogenesis.

The gene expression data obtained in the present study further supported the previously reported role of MWCNT-7 as a carcinogen in the rats (Kasai et al. 2016) and suggested mechanisms potentially underlying its carcinogenicity. The IPA biological function category, lung cancer, was significantly enriched in response to MWCNT-7 exposure in the rat lungs (Figure 8) similar to that reported by Guo et al. (2012) in mice exposed to MWCNT-7 by pharyngeal aspiration. Similarly, cell cycle control of chromosomal replication and kinetochore metaphase signaling pathway were two of the significantly enriched canonical pathway categories in the MWCNT-7 exposed rat lungs (Figure 8). The enrichment of these IPA categories and the over expression of the genes involved in those categories (Table 1), similar to the results of the lung toxicity assessment parameters employed in the study, were dependent on the MWCNT-7 dose to which the rats were exposed suggesting the potential involvement of the over expressed genes in mediating the MWCNT-7-induced lung toxicity/ carcinogenesis.

Faithful replication of chromosomal DNA is essential for stable propagation of the genetic information during cell division. This requires that chromosomal DNA replication, a very complex process, regulated by the expression of multiple genes, takes place only once per cell division. The genes that regulate the chromosomal DNA replication during cell division/ cycle belong to three major classes - origin recognition complex (ORC), minichromosome maintenance (MCM), and cell division cycle (CDC), each regulating distinct and critical events involved in the faithful replication of chromosomal DNA (Hizume et al. 2013; Dabral et al. 2019; Perl et al. 2019). Overexpression of the ORC, MCM, and CDC genes resulting in excessive production of the encoded proteins and modulation of their functions may result in abnormal chromosomal DNA replication leading to cell transformation and cancer (Semple and Duncker, 2004; Tomita et al. 2011; Issac et al. 2019). As presented in Table 1, members of the ORC, MCM, and CDC gene families were significantly overexpressed in the lungs of the MWCNT-7 exposed rats suggesting their potential involvement in lung cancer due to exposure to MWCNT-7.

Another major event in cell division, relevant to carcinogenesis, is replication of the chromosomes taking place during metaphase and their subsequent segregation, equally, during anaphase to result in daughter cells with the same number of chromosomes as the parental cell. The kinetochore-spindle assembly formation plays a critical role in the equal segregation of the sister chromatids to the daughter cells. The entire process is controlled by proteins that belong to the KMN network consisting of Knl1, Mis12, and Ndc80 complexes (Varma and Salmon 2012). Transcripts for the genes whose protein products play important roles in the kinetochore-spindle assembly formation, through their participation in the KMN network, were found significantly overexpressed in the MWCNT-7 exposed rat lungs

(Table 1). The established role of KMN genes in oncogenesis (Bai et al. 2019; Gao et al. 2021), the observation that MWCNT-7-induced aneuploidy resulted in the acquisition of an oncogenic phenotype in human airway epithelial cells (Siegrist et al. 2014), and the significant overexpression of the KMN network gene transcripts in the MWCNT-7 exposed rat lungs (Table 1) may suggest that deregulation of expression of the genes involved in kinetochore metaphase signaling pathway is a potential mechanism underlying MWCNT-7 induced cancer.

The transcriptomic data obtained in the present study may suggest that the molecular mechanisms underlying the lung toxicity of MWCNT-7 and other respirable, toxic particles exhibit considerable similarity despite the differences in their physicochemical properties. Many of the biological processes and pathways that were significantly enriched in response to the whole-body inhalation exposure of rats to MWCNT-7 were also found significantly enriched in response to pulmonary exposure of mouse to SWCNT (Fujita et al. 2015), and rats to CNC (Joseph et al. 2021), or crystalline silica (Sager et al. 2020). Similarly, the pathways that were significantly enriched in response to intratracheal (Poulsen et al. 2015), pharyngeal aspiration (Snyder-Talkington et al. 2013), and nose-only inhalation exposure (Seidel et al. 2021) to MWCNT exhibited considerable similarity. These findings, in agreement with the observations by Labib et al. (2016), may suggest the involvement of common molecular mechanisms underlying the lung toxicity of different particles that differ in their physicochemical properties despite the differences in the genes involved and their fold-changes in expression.

In conclusion, the whole-body inhalation exposure of rats to MWCNT-7 resulted in dose-dependent gene expression changes in their lungs. Bioinformatic analysis of the gene expression data provided information regarding the molecular mechanisms underlying the MWCNT-7-induced lung toxicity and its role as a carcinogen. Significant enrichment in biological processes and pathways related to pulmonary infiltration of phagocytes and their activation, reactive oxidant generation, induction of inflammation and fibrosis, and carcinogenesis were identified suggesting the involvement of these mechanisms in the lung toxicity and carcinogenesis of MWCNT-7 detected in animal models.

Acknowledgements

The authors thank Howard Leonard (NIOSH, Morgantown) for assistance with inhalation exposure of rats.

Funding

Funding for this project was provided by the NIOSH Nanotechnology Research Center (Project Numbers 921044E and 93909 NA).

References

Alfadda AA, Fatma S, Chishti MA, Al-Naami MY, Elawad R, Mendoza CD, Jo H, Lee YS. 2012. Orosomucoid serum concentrations and fat depot-specific mRNA and protein expression in humans. Mol Cells 33(1):35–41. [PubMed: 22134720]

Andrews S. 2010. FastQC: a quality control tool for high throughput sequence data http://www.bioinformatics.babraham.ac.uk/projects/fastqc.

Anjilvel S, Asgharian B. 1995. A multiple-path model of particle deposition in the rat lung. Fundam Appl Toxicol 28(1):41–50. [PubMed: 8566482]

Asakura M, Sasaki T, Sugiyama T, Takaya M, Koda S, Nagano K, Arito H, Fukushima S. 2010. Genotoxicity and cytotoxicity of multi-wall carbon nanotubes in cultured Chinese hamster lung cells in comparison with chrysotile A fibers. J Occup Health 52(3):155–166. [PubMed: 20379079]

Bai T, Zhao Y, Liu Y, Cai B, Dong N, Li B. 2019. Effect of KNL1 on the proliferation and apoptosis of colorectal cancer cells. Technol Cancer Res Treat 18:1533033819858668. [PubMed: 31315522]

Beard JD, Erdely A, Dahm MM, de Perio MA, Birch ME, Evans DE, Fernback JE, Eye T, Kodali V, Mercer RR, et al. 2018. Carbon nanotube and nanofiber exposure and sputum and blood biomarkers of early effect among U.S. workers. Environ Int 116:214–228. [PubMed: 29698898]

Becker S, Quay J, Soukup J. 1991. Cytokine (tumor necrosis factor, IL-6, and IL-8) production by respiratory syncytial virus-infected human alveolar macrophages. J Immunol 147(12):4307–4312. [PubMed: 1753101]

Bleharski JR, Kiessler V, Buonsanti C, Sieling PA, Stenger S, Colonna M, Modlin RL. 2003. A role for triggering receptor expressed on myeloid cells-1 in host defense during the early-induced and adaptive phases of the immune response. J Immunol 170(7):3812–3818. [PubMed: 12646648]

Bolger AM, Lohse M, Usadel B. 2014. Trimmomatic: a flexible trimmer for Illumina sequence data. Bioinformatics 30(15):2114–2120. [PubMed: 24695404]

Butler C. 1976. Lung surface area in various morphologic forms of human emphysema. Am Rev Respir Dis 114(2):347–352. [PubMed: 973726]

Castranova V. 1994. Generation of oxygen radicals and mechanisms of injury prevention. Environ Health Perspect 102(Suppl 10):65–68.

Chen T, Yang J, Ren G, Yang Z, Zhang T. 2013. Multi-walled carbon nanotube increases the excitability of hippocampal CA1 neurons through inhibition of potassium channels in rat's brain slices. Toxicol Lett 217(2):121–128. [PubMed: 23274715]

Chen TY, Zhou M, Lin MQ, Liang ST, Yan Y, Wang SM, Fang CS, Li D, Ruan Y. 2021. Research progress on the SERPINE1 protein and chronic inflammatory diseases of the upper respiratory tract: a literature review. Int Arch Allergy Immunol 182(11):1097–1102. [PubMed: 33946071]

Churg A, Wright JL. 2005. Proteases and emphysema. Curr Opin Pulm Med 11(2):153–159. [PubMed: 15699789]

Cronstein BN. 2011. Adenosine receptors and fibrosis: a translational review. F1000 Biol Rep 3:21. [PubMed: 22003368]

Dabral P, Uppal T, Rossetto CC, Verma SC. 2019. Minichromosome maintenance proteins cooperate with LANA during the G1/S phase of the cell cycle to support viral DNA replication. J Virol 93(7): e02256–18. [PubMed: 30651368]

Dahm MM, Evans DE, Schubauer-Berigan MK, Birch ME, Fernback JE. 2012. Occupational exposure assessment in carbon nanotube and nanofiber primary and secondary manufacturers. Ann Occup Hyg 56:542–556. [PubMed: 22156567]

Dahm MM, Schubauer-Berigan MK, Evans DE, Birch ME, Bertke S, Beard JD, Erdely A, Fernback JE, Mercer RR, Grinshpun SA. 2018. Exposure assessments for a cross-sectional epidemiologic study of US carbon nanotube and nanofiber workers. Int J Hyg Environ Health 221(3):429–440. [PubMed: 29339022]

Delorme MP, Muro Y, Arai T, Banas DA, Frame SR, Reed KL, Warheit DB. 2012. Ninety-day inhalation toxicity study with a vapor grown carbon nanofiber in rats. Toxicol Sci 128(2):449–460. [PubMed: 22581831]

Donaldson K, Aitken R, Tran L, Stone V, Duffin R, Forrest G, Alexander A. 2006. Carbon nanotubes: a review of their properties in relation to pulmonary toxicology and workplace safety. Toxicol Sci 92(1):5–22. [PubMed: 16484287]

Donaldson K, Poland CA, Murphy FA, MacFarlane M, Chernova T, Schinwald A. 2013. Pulmonary toxicity of carbon nanotubes and asbestos – similarities and differences. Adv Drug Deliv Rev 65(15): 2078–2086. [PubMed: 23899865]

Dong J, Ma Q. 2016a. Suppression of basal and carbon nanotube-induced oxidative stress, inflammation and fibrosis in mouse lungs by Nrf2. Nanotoxicology 10(6):699–709. [PubMed: 26592091]

Dong J, Ma Q. 2016b. TIMP1 promotes multi-walled carbon nanotube-induced lung fibrosis by stimulating fibroblast activation and proliferation. Nanotoxicology 11(1):41–11. [PubMed: 27852133]

Dong J, Ma Q. 2017. Osteopontin enhances multi-walled carbon nanotube-triggered lung fibrosis by promoting TGF-b1 activation and myofibroblast differentiation . Part Fibre Toxicol 14(1):18. [PubMed: 28595626]

Dong J, Porter DW, Batteli LA, Wolfarth MG, Richardson DL, Ma Q. 2015. Pathologic and molecular profiling of rapid-onset fibrosis and inflammation induced by multi-walled carbon nanotubes. Arch Toxicol 89(4):621–633. [PubMed: 25510677]

Dymacek JM, Snyder-Talkington BN, Raese R, Dong C, Singh S, Porter DW, Ducatman B, Wolfarth MG, Andrew ME, Battelli L, et al. 2018. Similar and differential canonical pathways and biological processes associated with multiwalled carbon nanotube and asbestos-induced pulmonary fibrosis: a 1-year postexposure study. Int J Toxicol 37(4):276–284. [PubMed: 29916280]

Eatemadi A, Daraee H, Karimkhanloo H, Kouhi M, Zarghami N, Akbarzadeh A, Abasi M, Hanifehpour Y, Joo SW. 2014. Carbon nanotubes: properties, synthesis, purification, and medical applications. Nanoscale Res Lett 9(1):393. [PubMed: 25170330]

Ema M, Imamura T, Suzuki H, Kobayashi N, Naya M, Nakanishi J. 2012. Evaluation of genotoxicity of multi-walled carbon nanotubes in a battery of *in vitro* and *in vivo* assays. Regul Toxicol Pharmacol 63(2):188–195. [PubMed: 22504735]

Erdely A, Dahm M, Chen BT, Zeidler-Erdely PC, Fernback JE, Birch ME, Evans DE, Kashon ML, Deddens JA, Hulderman T, et al. 2013. Carbon nanotube dosimetry: from workplace exposure assessment to inhalation toxicology. Part Fibre Toxicol 10(1):53. [PubMed: 24144386]

Fatkhutdinova LM, Khaliullin TO, Vasil'yeva OL, Zalyalov RR, Mustafin IG, Kisin ER, Birch ME, Yanamala N, Shvedova AA. 2016. Fibrosis biomarkers in workers exposed to MWCNTs. Toxicol Appl Pharmacol 299:125–131. [PubMed: 26902652]

Fenoglio I, Tomatis M, Lison D, Muller J, Fonseca A, Nagy JB, Fubini B. 2006. Reactivity of carbon nanotubes: free radical generation or scavenging activity? Free Radic Biol Med 40(7):1227–1233. [PubMed: 16545691]

Fubini B, Bolis V, Giamello E, Volante M. 1991. Chemical functionalities at the broken fibre surface relatable to free radicals production. In: Brown RC, Hoskins JA, Johnson NF, editors. Mechanisms in fibre carcinogenesis New York: Plenum Press.

Fujita K, Fukuda M, Fukui H, Horie M, Endoh S, Uchida K, Shichiri M, Morimoto Y, Ogami A, Iwahashi H. 2015. Intratracheal instillation of single-wall carbon nanotubes in the rat lung induces time-dependent changes in gene expression. Nanotoxicology 9(3): 290–301. [PubMed: 24911292]

Fukushima S, Kasai T, Umeda Y, Ohnishi M, Sasaki T, Matsumoto M. 2018. Carcinogenicity of multi-walled carbon nanotubes: challenging issue on hazard assessment. J Occup Health 60(1):10–30. [PubMed: 29046510]

Gao H, Pan QY, Wang YJ, Chen QF. 2021. Impact of KMN network genes on progression and prognosis of non-small cell lung cancer. Anticancer Drugs 33(1):e398–e408.

Gate L, Knudsen KB, Seidel C, Berthing T, Chezeau L, Jacobsen NR, Valentino S, Wallin H, Bau S, Wolff H, et al. 2019. Toxicol Appl Pharmacol 375:17–31. [PubMed: 31075343]

Ghosh AK, Vaughan DE. 2012. PAI-1 in tissue fibrosis. J Cell Physiol 227(2):493–507. [PubMed: 21465481]

Guo NL, Wan YW, Denvir J, Porter DW, Pacurari M, Wolfarth MG, Castranova V, Qian Y. 2012. Multiwalled carbon nanotube-induced gene signatures in the mouse lung: potential predictive value for human lung cancer risk and prognosis. J Toxicol Environ Health A 75(18):1129–1153. [PubMed: 22891886]

Hamadeh HK, Bushel PR, Jayadev S, Martin K, DiSorbo O, Sieber S, Bennett L, Tennant R, Stoll R, Barrett JC, et al. 2002. Gene expression analysis reveals chemical-specific profiles. Toxicol Sci 67(2): 219–231. [PubMed: 12011481]

Heinloth AN, Irwin RD, Boorman GA, Nettesheim P, Fannin RD, Sieber SO, Snell ML, Tucker CJ, Li L, Travlos GS, et al. 2004. Gene expression profiling of rat livers reveals indicators of potential adverse effects. Toxicol Sci 80(1):193–202. [PubMed: 15084756]

Hizume K, Yagura M, Araki H. 2013. Concerted interaction between origin recognition complex (ORC), nucleosomes and replication origin DNA ensures stable ORC-origin binding. Genes Cells 18(9): 764–779. [PubMed: 23795651]

Huang WT, Vayalil PK, Miyata T, Hagood J, Liu RM. 2012. Therapeutic value of small molecule inhibitor to plasminogen activator inhibitor-1 for lung fibrosis. Am J Respir Cell Mol Biol 46(1): 87–95. [PubMed: 21852684]

Huber-Lang M, Younkin EM, Sarma JV, Riedemann N, McGuire SR, Lu KT, Kunkel R, Younger JG, Zetoune FS, Ward PA. 2002. Generation of C5a by phagocytic cells. Am J Pathol 161(5): 1849–1859. [PubMed: 12414531]

IARC (International Agency for Research on Cancer). 2017. Some nanomaterials and some fibers Lyon, France: International Agency for Research on Cancer.

Issac MSM, Yousef E, Tahir MR, Gaboury LA. 2019. MCM2, MCM4, and MCM6 in breast cancer: clinical utility in diagnosis and prognosis. Neoplasia 21(10):1015–1035. [PubMed: 31476594]

Joseph P. 2017. Transcriptomics in toxicology. Food Chem Toxicol 109(Pt 1):650–662. [PubMed: 28720289]

Joseph P, Umbright CM, Roberts JR, Cumpston JL, Orandle MS, McKinney WG, Sager TM. 2021. Lung toxicity and gene expression changes in response to whole-body inhalation exposure to cellulose nanocrystal in rats. Inhal Toxicol 33(2):66–80. [PubMed: 33602020]

Kasai T, Umeda Y, Ohnishi M, Kondo H, Takeuchi T, Aiso S, Nishizawa T, Matsumoto M, Fukushima S. 2015. Thirteen-week study of toxicity of fiber-like multi-walled carbon nanotubes with whole-body inhalation exposure in rats. Nanotoxicology 9(4): 413–422. [PubMed: 25030099]

Kasai T, Umeda Y, Ohnishi M, Mine T, Kondo H, Takeuchi T, Matsumoto M, Fukushima S. 2016. Lung carcinogenicity of inhaled multi-walled carbon nanotube in rats. Part Fibre Toxicol 13(1):53. [PubMed: 27737701]

Katsuyama M, Matsuno K, Yabe-Nishimura C. 2012. Physiological roles of NOX/NADPH oxidase, the superoxide-generating enzyme. J Clin Biochem Nutr 50(1):9–22. [PubMed: 22247596]

Kensler TW, Wakabayashi N, Biswal S. 2007. Cell survival responses to environmental stresses via the Keap1-Nrf2-ARE pathway. Annu Rev Pharmacol Toxicol 47:89–116. [PubMed: 16968214]

Kim D, Langmead B, Salzberg SL. 2015. HISAT: a fast spliced aligner with low memory requirements. Nat Methods 12(4):357–360. [PubMed: 25751142]

Labib S, Williams A, Yauk CL, Nikota JK, Wallin H, Vogel U, Halappanavar S. 2016. Nano-risk science: application of toxicogenomics in an adverse outcome pathway framework for risk assessment of multi-walled carbon nanotubes. Part Fibre Toxicol 13:15. [PubMed: 26979667]

Laskin DL, Laskin JD. 2001. Role of macrophages and inflammatory mediators in chemically induced toxicity. Toxicology 160(1–3): 111–118. [PubMed: 11246131]

Law CW, Alhamdoosh M, Su S, Dong X, Tian L, Smyth GK, Ritchie ME. 2016. RNA-seq analysis is easy as 1–2-3 with limma, Glimma and edgeR. F1000Res 5:1408.

Lee CG, Herzog EL, Ahangari F, Zhou Y, Gulati M, Lee CM, Peng X, Feghali-Bostwick C, Jimenez SA, Varga J, et al. 2012. Chitinase 1 is a biomarker for and therapeutic target in scleroderma-associated interstitial lung disease that augments TGF-b1 signaling. J Immunol 189(5):2635–2644. [PubMed: 22826322]

Lee JS, Choi YC, Shin JH, Lee JH, Lee Y, Park SY, Baek JE, Park JD, Ahn K, Yu IJ. 2015. Health surveillance study of workers who manufacture multi-walled carbon nanotubes. Nanotoxicology 9(6): 802–811. [PubMed: 25395166]

Li H, Handsaker B, Wysoker A, Fennell T, Ruan J, Homer N, Marth G, Abecasis G, Durbin R, Genome Project Data Processing S, 1000 Genome Project Data Processing Subgroup. 2009. The Sequence alignment/map format and SAMtools. Bioinformatics 25(16): 2078–2079. [PubMed: 19505943]

Ligresti G, Aplin AC, Dunn BE, Morishita A, Nicosia RF. 2012. The acute phase reactant orosomucoid-1 is a bimodal regulator of angiogenesis with time- and context-dependent inhibitory and stimulatory properties. PLOS One 7(8):e41387. [PubMed: 22916107]

Ma-Hock L, Treumann S, Strauss V, Brill S, Luizi F, Mertler M, Wiench K, Gamer AO, van Ravenzwaay B, Landsiedel R. 2009. Inhalation toxicity of multiwall carbon nanotubes in rats exposed for 3 months. Toxicol Sci 112(2):468–481. [PubMed: 19584127]

McKinney W, Chen B, Frazer D. 2009. Computer controlled multi-walled carbon nanotube inhalation exposure system. Inhal Toxicol 21(12):1053–1061. [PubMed: 19555230]

McKinney W, Chen B, Schwegler-Berry D, Frazer DG. 2013. Computer-automated silica aerosol generator and animal inhalation exposure system. Inhal Toxicol 25(7):363–372. [PubMed: 23796015]

Mercer RR, Hubbs AF, Scabilloni JF, Wang L, Battelli LA, Schwegler-Berry D, Castranova V, Porter DW. 2010. Distribution and persistence of pleural penetrations by multi-walled carbon nanotubes. Part Fibre Toxicol 7:28. [PubMed: 20920331]

Mercer RR, Scabilloni JF, Hubbs AF, Battelli LA, McKinney W, Friend S, Wolfarth MG, Andrew M, Castranova V, Porter DW. 2013. Distribution and fibrotic response following inhalation exposure to multi-walled carbon nanotubes. Part Fibre Toxicol 10:33. [PubMed: 23895460]

Mizgerd JP. 2002. Molecular mechanisms of neutrophil recruitment elicited by bacteria in the lungs. Semin Immunol 14(2):123–132. [PubMed: 11978084]

Muller J, Huaux F, Moreau N, Misson P, Heilier JF, Delos M, Arras M, Fonseca A, Nagy JB, Lison D. 2005. Respiratory toxicity of multi-wall carbon nanotubes. Toxicol Appl Pharmacol 207(3): 221–231. [PubMed: 16129115]

Nair MG, Du Y, Perrigoue JG, Zaph C, Taylor JJ, Goldschmidt M, Swain GP, Yancopoulos GD, Valenzuela DM, Murphy A, et al. 2009. Alternatively activated macrophage-derived RELM-{alpha} is a negative regulator of type 2 inflammation in the lung. J Exp Med 206(4):937–952. [PubMed: 19349464]

Nakashima K, Sato T, Shigemori S, Shimosato T, Shinkai M, Kaneko T. 2018. Regulatory role of heme oxygenase-1 in silica-induced lung injury. Respir Res 19(1):144. [PubMed: 30068325]

Nikota J, Williams A, Yauk CL, Wallin H, Vogel U, Halappanavar S. 2016. Meta-analysis of transcriptomic responses as a means to identify pulmonary disease outcomes for engineered nanomaterials. Part Fibre Toxicol 13(1):25. [PubMed: 27169501]

NIOSH (National Institute for Occupational Safety and Health). 2013. Current intelligence bulletin 65: occupational exposure to carbon nanotubes and nanofibers Cincinnati, Ohio: US Department of Health and Human Services Centers for Disease Control and Prevention, National Institute for Occupational Safety and Health (2013. Publication No. 2013–145).

NRC (National Research Council). 2007. Toxicity testing in the 21st century: a vision and a strtegy Washington, DC: The National Academies Press.

Numano T, Higuchi H, Alexander DB, Alexander WT, Abdelgied M, El-Gazzar AM, Saleh D, Takase H, Hirose A, Naiki-Itop A, et al. 2019. MWCNT-7 administered to the lung by intratracheal instillation induces development of pleural mesothelioma in F344 rats. Cancer Sci 110(8):2485–2492. [PubMed: 31265162]

Ohashi T, Pinkerton K, Ikegami M, Jobe AH. 1994. Changes in alveolar surface area, surfactant protein A, and saturated phosphatidylcholine with postnatal rat lung growth. Pediatr Res 35(6):685–689. [PubMed: 7936819]

Ornatowska M, Azim AC, Wang X, Christman JW, Xiao L, Joo M, Sadikot RT. 2007. Functional genomics of silencing TREM-1 on TLR4 signaling in macrophages. Am J Physiol Lung Cell Mol Physiol 293(6):L1377–1384. [PubMed: 17905855]

Pandya PH, Wilkes DS. 2014. Complement system in lung disease. Am J Respir Cell Mol Biol 51(4):467–473. [PubMed: 24901241]

Perez L. 2019. Acute phase protein response to viral infection and vaccination. Arch Biochem Biophys 671:196–202. [PubMed: 31323216]

Perl AL, O'Connor CM, Fa P, Mayca Pozo F, Zhang J, Zhang Y, Narla G. 2019. Protein phosphatase 2A controls ongoing DNA replication by binding to and regulating cell division cycle 45 (CDC45). J Biol Chem 294(45):17043–17059. [PubMed: 31562245]

Pilling D, Cox N, Vakil V, Verbeek JS, Gomer RH. 2015. The long pentraxin PTX3 promotes fibrocyte differentiation. PLOS One 10(3):e0119709. [PubMed: 25774777]

Porter DW, Hubbs AF, Chen BT, McKinney W, Mercer RR, Wolfarth MG, Battelli L, Wu N, Sriram K, Leonard S, et al. 2013. Acute pulmonary dose-responses to inhaled multi-walled carbon nanotubes. Nanotoxicology 7(7):1179–1194. [PubMed: 22881873]

Porter DW, Hubbs AF, Mercer RR, Wu N, Wolfarth MG, Sriram K, Leonard S, Battelli L, Schwegler-Berry D, Friend S, et al. 2010. Mouse pulmonary dose- and time course-responses induced by exposure to multi-walled carbon nanotubes. Toxicology 269(2–3): 136–147. [PubMed: 19857541]

Poulsen SS, Jackson P, Kling K, Knudsen KB, Skaug V, Kyjovska ZO, Thomsen BL, Clausen PA, Atluri R, Berthing T, et al. 2016. Multi-walled carbon nanotube physicochemical properties predict pulmonary inflammation and genotoxicity. Nanotoxicology 10(9): 1263–1275. [PubMed: 27323647]

Poulsen SS, Saber AT, Williams A, Andersen O, Kobler C, Atluri R, Pozzebon ME, Mucelli SP, Simion M, Rickerby D, et al. 2015. MWCNTs of different physicochemical properties cause similar inflammatory responses, but differences in transcriptional and histological markers of fibrosis in mouse lungs. Toxicol Appl Pharmacol 284(1):16–32. [PubMed: 25554681]

R Core Team. 2018. R: a language and environment for statistical computing Vienna, Austria: R Foundation for Statistical Computing.

Roberts JR, Anderson SE, Kan H, Krajnak K, Thompson JA, Kenyon A, Goldsmith WT, McKinney W, Frazer DG, Jackson M, et al. 2014. Evaluation of pulmonary and systemic toxicity of oil dispersant (COREXIT EC9500A((R))) following acute repeated inhalation exposure. Environ Health Insights 8(Suppl 1):63–74. [PubMed: 25861220]

Roudkenar MH, Kuwahara Y, Baba T, Roushandeh AM, Ebishima S, Abe S, Ohkubo Y, Fukumoto M. 2007. Oxidative stress induced lipocalin 2 gene expression: addressing its expression under the harmful conditions. J Radiat Res 48(1):39–44. [PubMed: 17229997]

Ryman-Rasmussen JP, Cesta MF, Brody AR, Shipley-Phillips JK, Everitt JI, Tewksbury EW, Moss OR, Wong BA, Dodd DE, Andersen ME, et al. 2009. Inhaled carbon nanotubes reach the subpleural tissue in mice. Nat Nanotechnol 4(11):747–751. [PubMed: 19893520]

Saber AT, Jacobsen NR, Jackson P, Poulsen SS, Kyjovska ZO, Halappanavar S, Yauk CL, Wallin H, Vogel U. 2014. Particle-induced pulmonary acute phase response may be the causal link between particle inhalation and cardiovascular disease. Wiley Interdiscip Rev Nanomed Nanobiotechnol 6(6):517–531. [PubMed: 24920450]

Sack GH. Jr., 2018. Serum amyloid A – a review. Mol Med 24(1):46. [PubMed: 30165816]

Sager TM, Umbright CM, Mustafa GM, Yanamala N, Leonard HD, McKinney WG, Kashon ML, Joseph P. 2020. Tobacco smoke exposure exacerbated crystalline silica-induced lung toxicity in rats. Toxicol Sci 178(2):375–390. [PubMed: 32976597]

Sakamoto Y, Nakae D, Fukumori N, Tayama K, Maekawa A, Imai K, Hirose A, Nishimura T, Ohashi N, Ogata A. 2009. Induction of mesothelioma by a single intrascrotal administration of multi-wall carbon nanotube in intact male Fischer 344 rats. J Toxicol Sci 34(1):65–76. [PubMed: 19182436]

Saleh DM, Alexander WT, Numano T, Ahmed OHM, Gunasekaran S, Alexander DB, Abdelgied M, El-Gazzar AM, Takase H, Xu J, et al. 2020. Comparative carcinogenicity study of a thick, straight-type and a thin, tangled-type multi-walled carbon nanotube administered by intra-tracheal instillation in the rat. Part Fibre Toxicol 17(1):48. [PubMed: 33054855]

Sargent LM, Porter DW, Staska LM, Hubbs AF, Lowry DT, Battelli L, Siegrist KJ, Kashon ML, Mercer RR, Bauer AK, et al. 2014. Promotion of lung adenocarcinoma following inhalation exposure to multi-walled carbon nanotubes. Part Fibre Toxicol 11:3. [PubMed: 24405760]

Seidel C, Zhernovkov V, Cassidy H, Kholodenko B, Matallanas D, Cosnier F, Gate L. 2021. Inhaled multi-walled carbon nanotubes differently modulate global gene and protein expression in rat lungs. Nanotoxicology 15(2):238–256. [PubMed: 33332178]

Semple JW, Duncker BP. 2004. ORC-associated replication factors as biomarkers for cancer. Biotechnol Adv 22(8):621–631. [PubMed: 15364349]

Sharma S, Singh AK, Kaushik S, Sinha M, Singh RP, Sharma P, Sirohi H, Kaur P, Singh TP. 2013. Lactoperoxidase: structural insights into the function, ligand binding and inhibition. Int J Biochem Mol Biol 4(3):108–128. [PubMed: 24049667]

Siegrist KJ, Reynolds SH, Kashon ML, Lowry DT, Dong C, Hubbs AF, Young SH, Salisbury JL, Porter DW, Benkovic SA, et al. 2014. Genotoxicity of multi-walled carbon nanotubes at occupationally relevant doses. Part Fibre Toxicol 11:6. [PubMed: 24479647]

Snyder-Talkington BN, Dymacek J, Porter DW, Wolfarth MG, Mercer RR, Pacurari M, Denvir J, Castranova V, Qian Y, Guo NL. 2013. System-based identification of toxicity pathways associated

with multi-walled carbon nanotube-induced pathological responses. Toxicol Appl Pharmacol 272(2):476–489. [PubMed: 23845593]

Stapleton PA, Minarchick VC, Cumpston AM, McKinney W, Chen BT, Sager TM, Frazer DG, Mercer RR, Scabilloni J, Andrew ME, et al. 2012. Impairment of coronary arteriolar endothelium-dependent dilation after multi-walled carbon nanotube inhalation: a time-course study. Int J Mol Sci 13(11):13781–13803. [PubMed: 23203034]

Stoner BR, Brown B, Glass JT. 2014. Selected topics on the synthesis, properties and applications of multiwalled carbon nanotubes. Diam Relat Mater 42:49–57. [PubMed: 24910503]

Strunk RC, Eidlen DM, Mason RJ. 1988. Pulmonary alveolar type II epithelial cells synthesize and secrete proteins of the classical and alternative complement pathways. J Clin Invest 81(5):1419–1426. [PubMed: 2966814]

Takagi A, Hirose A, Nishimura T, Fukumori N, Ogata A, Ohashi N, Kitajima S, Kanno J. 2008. Induction of mesothelioma in p53+/−mouse by intraperitoneal application of multi-wall carbon nanotube. J Toxicol Sci 33(1):105–116. [PubMed: 18303189]

Tiwari N, Marudamuthu AS, Tsukasaki Y, Ikebe M, Fu J, Shetty S. 2016. p53- and PAI-1-mediated induction of C-X-C chemokines and CXCR2: importance in pulmonary inflammation due to cigarette smoke exposure. Am J Physiol Lung Cell Mol Physiol 310(6): L496–506. [PubMed: 26747783]

Tomita Y, Imai K, Senju S, Irie A, Inoue M, Hayashida Y, Shiraishi K, Mori T, Daigo Y, Tsunoda T, et al. 2011. A novel tumor-associated antigen, cell division cycle 45-like can induce cytotoxic T-lymphocytes reactive to tumor cells. Cancer Sci 102(4):697–705. [PubMed: 21231984]

Umeda Y, Kasai T, Saito M, Kondo H, Toya T, Aiso S, Okuda H, Nishizawa T, Fukushima S. 2013. Two-week toxicity of multi-walled carbon nanotubes by whole-body inhalation exposure in rats. J Toxicol Pathol 26(2):131–140. [PubMed: 23914055]

Varma D, Salmon ED. 2012. The KMN protein network-chief conductors of the kinetochore orchestra. J Cell Sci 125(Pt 24):5927–5936. [PubMed: 23418356]

Varsano S, Kaminsky M, Kaiser M, Rashkovsky L. 2000. Generation of complement C3 and expression of cell membrane complement inhibitory proteins by human bronchial epithelium cell line. Thorax 55(5):364–369. [PubMed: 10770816]

Volanakis JE. 1995. Transcriptional regulation of complement genes. Annu Rev Immunol 13:277–305. [PubMed: 7612224]

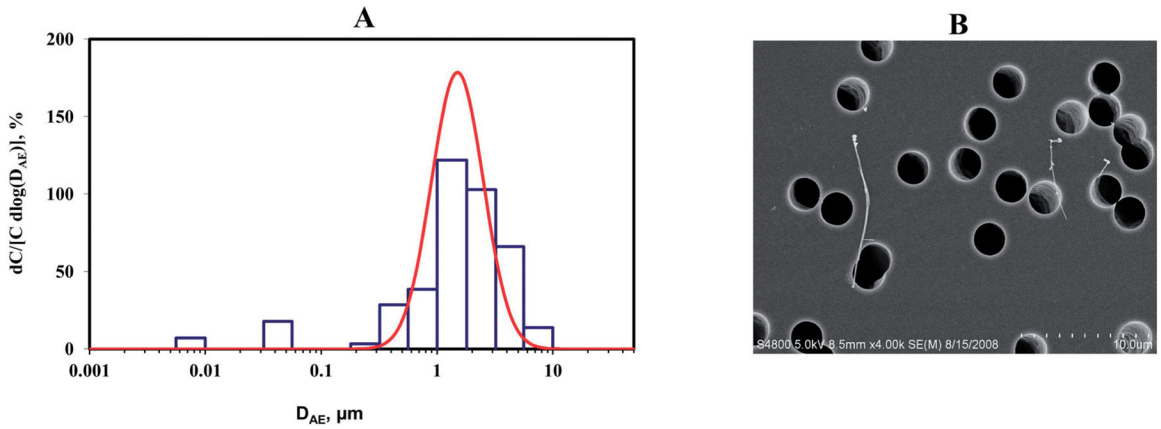

Figure 1.

Size distribution and morphology of MWCNT-7 particles in the aerosol generated for rat whole-body inhalation exposure. An aerosol containing MWCNT-7 particles was generated and used for inhalation exposure of rats. The aerosol generated was analyzed for particle size distribution using a MOUDI (A) and for particle size using an electron microscope (B) as described in the text. DAE: aerodynamic diameter; dC: concentration on each MOUDI stage; C: total concentration on all MOUDI stages.

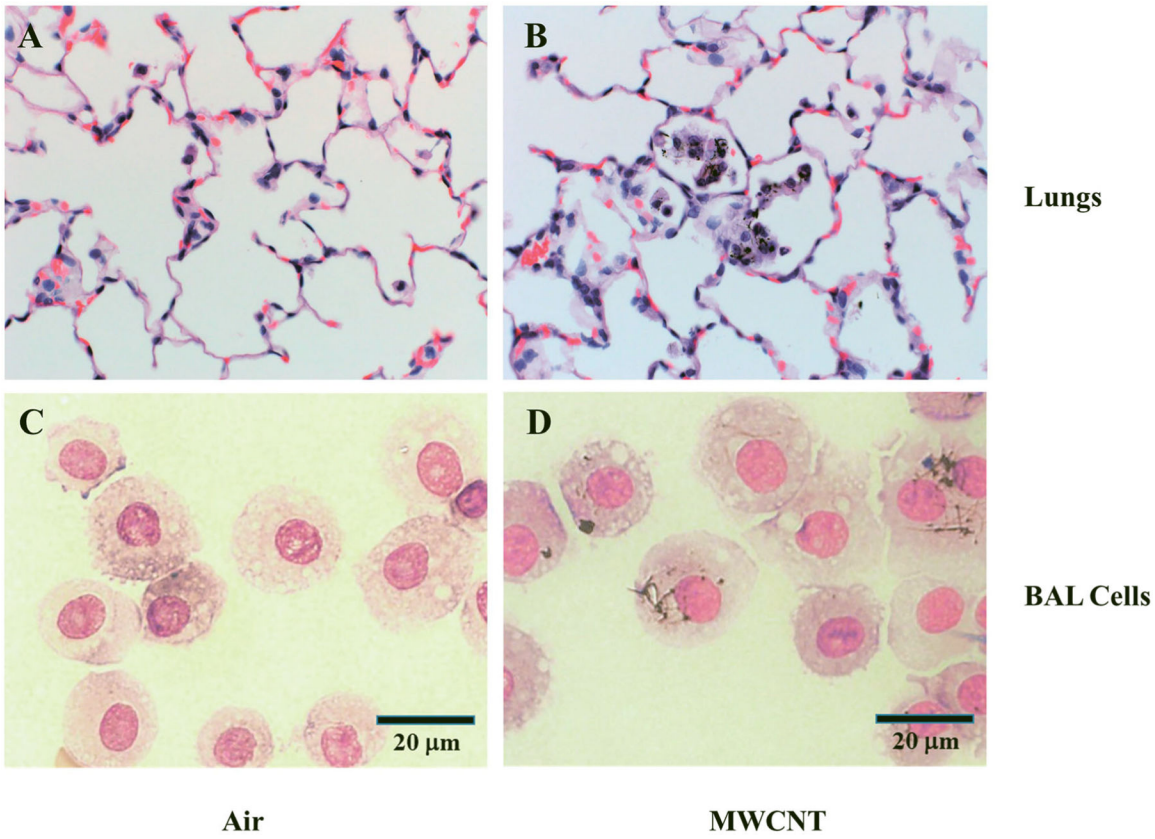

Figure 2.

Deposition of MWCNT-7 particles in rat lungs and uptake by alveolar macrophages. Rats were exposed by whole body inhalation to air, or an aerosol containing MWCNT-7 and euthanized as described in detail in the text. Sections of unlavaged right lung lobes prepared were observed under a light microscope to detect MWCNT-7 particles deposited in the lungs. Similarly, microscope slides containing BAL cells obtained following lavage of the left lungs were observed under a light microscope to detect MWCNT-7 particles (indicated by arrows in figure D). The lung sections and BAL samples obtained from rats exposed to air or 90 (mg/m^3)h MWCNT are presented as representatives.

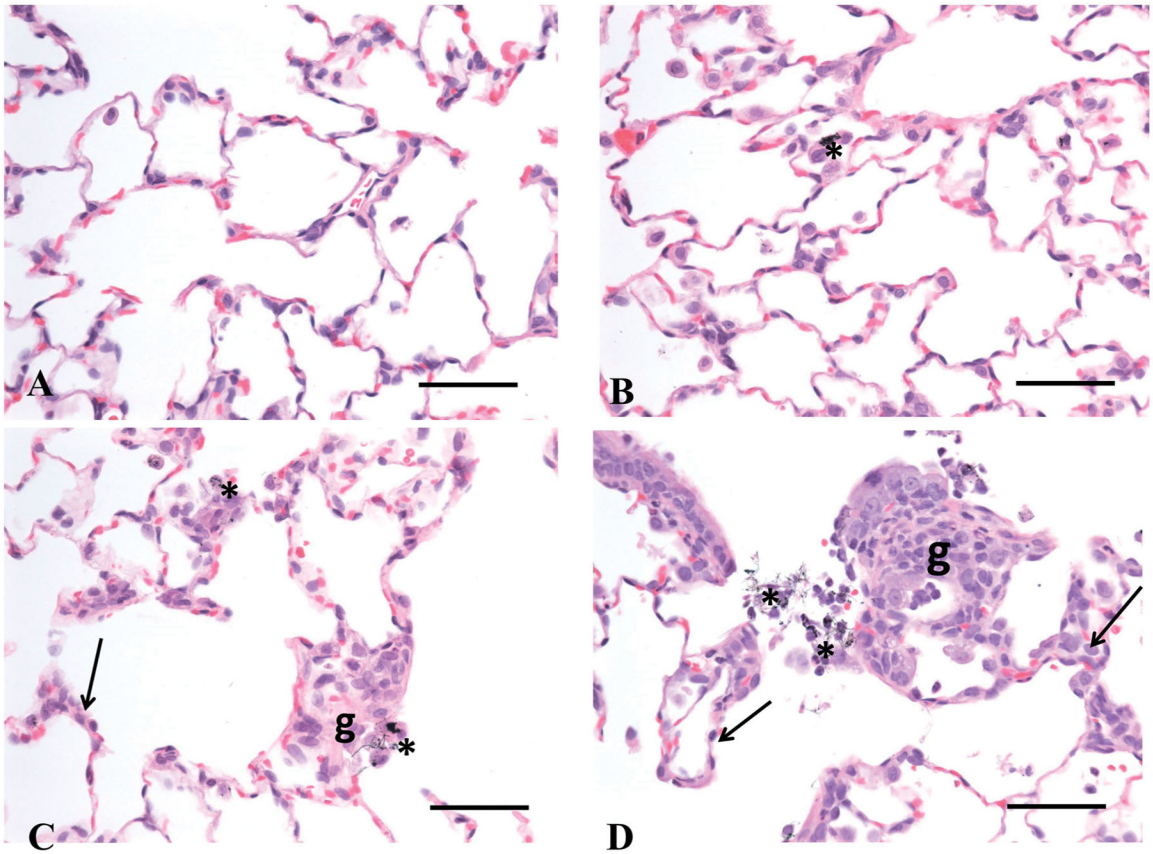

Figure 3.

Photomicrographs of lung sections from the control (air) and MWCNT-7 exposed rats. Lung sections prepared following euthanasia of the air or MWCNT-7 exposed rats were stained with hematoxylin and eosin and observed under a light microscope. Lungs of the air exposed rats showed normal histology (A). Except for occasional accumulation of pigmented nanoparticles in the alveolar lumina or inside macrophages (asterisk), no parenchymal changes were seen with the lower dose group of 45 (mg/m^3)h (B). With higher doses [90 (mg/m^3)h (C) and 180 (mg/m^3)h (D)], early alveolitis, seen as mild alveolar wall thickening and increased cellularity was noted (arrows), together with the presence of very early intra-alveolar granulomas (g) and numerous deposits of black pigmented MWCNT-7 particles (asterisk). The parenchymal changes were more obvious in the highest dose group (D). In all panels, bar = 50 μm and magnification = 40×.

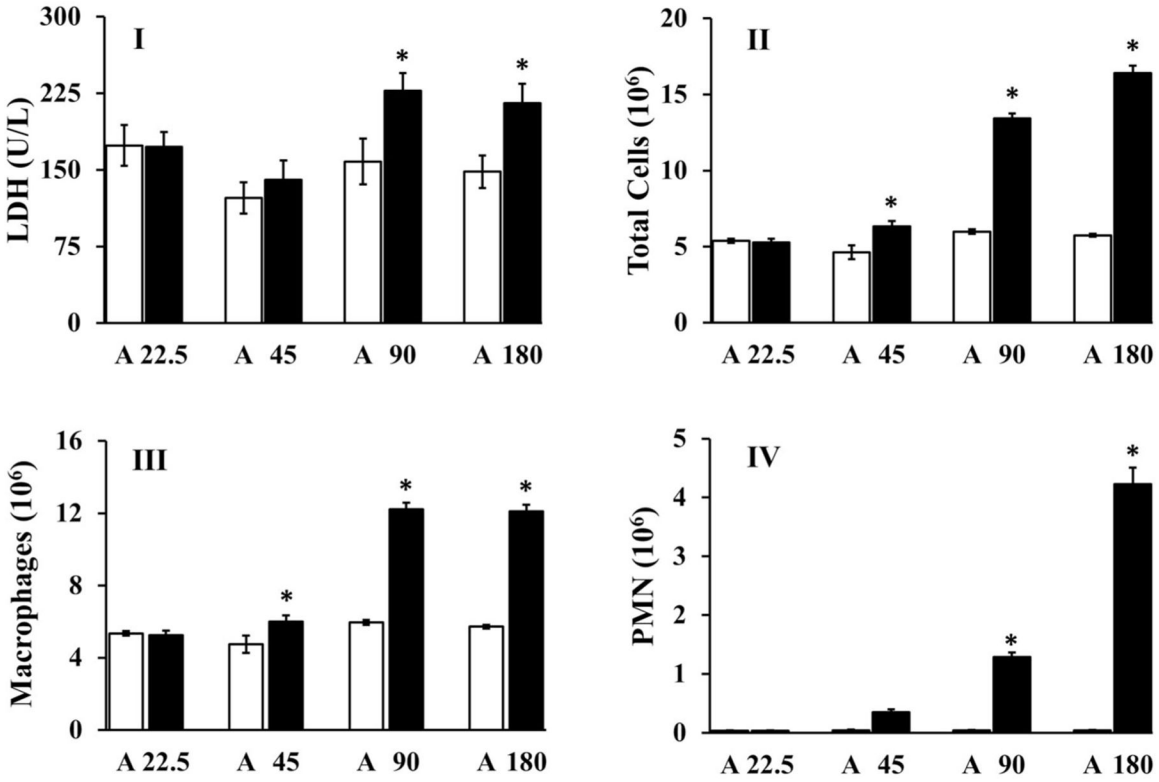

Figure 4.

Bronchoalveolar lavage parameters of toxicity in the rat lungs. The lungs of the control and MWCNT-7 exposed rats were lavaged and BAL cells and BAL fluid were isolated and analyzed for BAL parameters of toxicity, viz. LDH (I), total BAL cells (II), macrophages (III) and (PMN (IV).The filled and open bars correspond to the MWCNT-7 exposed and the respective control (air) groups of rats. The asterisk represents the statistical significance of the difference ($p < 0.05$) between the MWCNT-7 exposed and the corresponding control groups ($n = 12$).

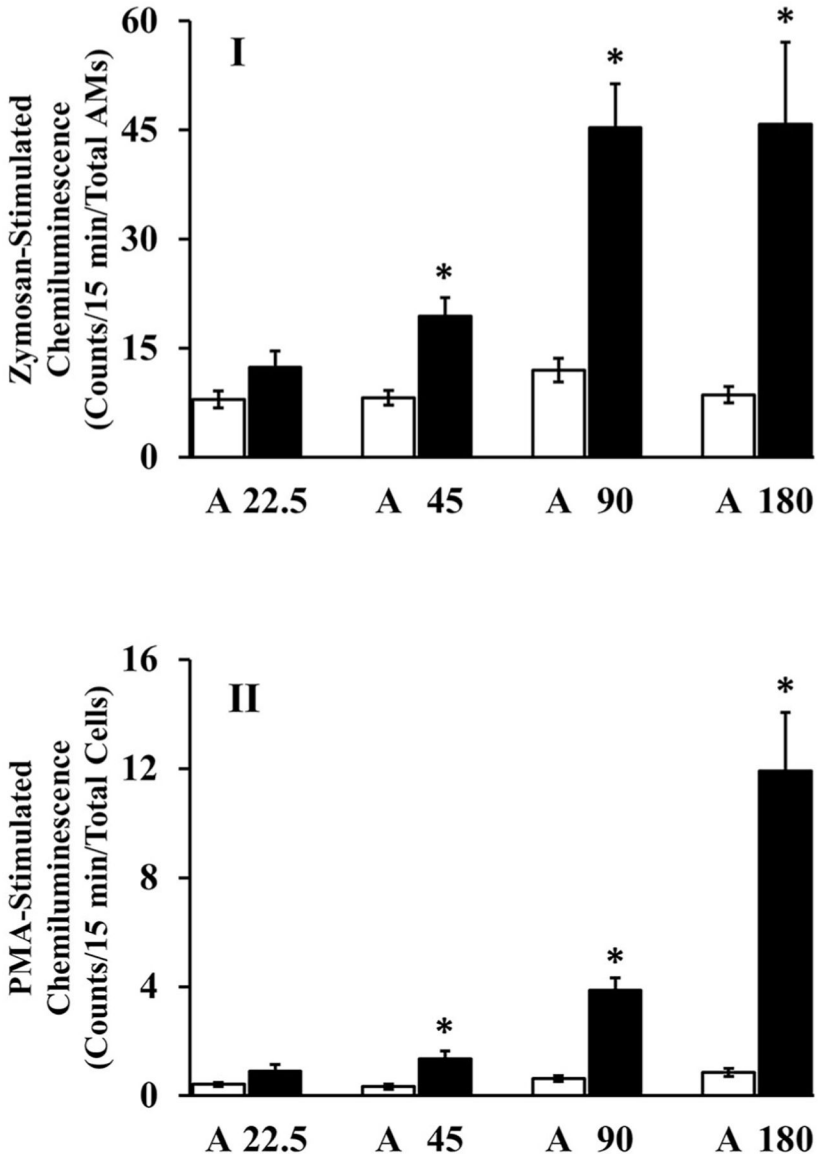

Figure 5.

Intracellular oxidants generated by the lung phagocytes in rats. The BAL cells obtained from the air or MWCNT-7 exposed rat lungs, following euthanasia, were analyzed for chemiluminescence representing the generation of intracellular reactive oxidants. Intracellular oxidants generated by the AMs only (I) and AMs and PMNs (II) are presented in the MWCNT exposed (filled bar) and corresponding control groups (A, open bar). The asterisk represents the statistical significance of the difference ($p < 0.05$) between the MWCNT-7 exposed and the corresponding control groups ($n = 12$).

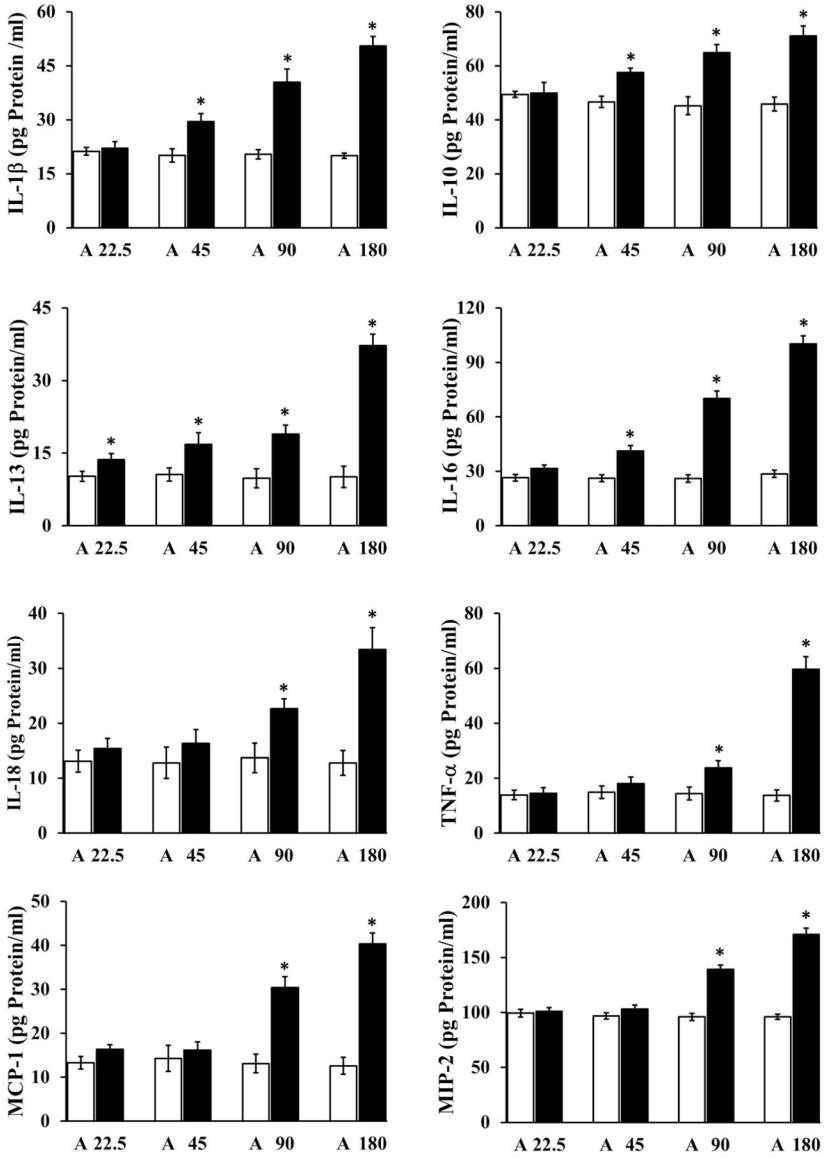

Figure 6.

Cytokine analysis in the lungs of the rats. The BAL fluid samples obtained from the air or MWCNT exposed lungs, following euthanasia of the rats, were analyzed and the protein corresponding to the individual cytokines were quantified by ELISA. The filled and open bars represent the MWCNT-7 exposed and the corresponding air exposed control (A) groups of rats, respectively. Data is presented as mean ± S.E. ($n = 5$ or 6) and the asterisks represent the statistical significance ($p < 0.05$) of the data between the MWCNT-7 exposed and the corresponding air exposed groups of rats.

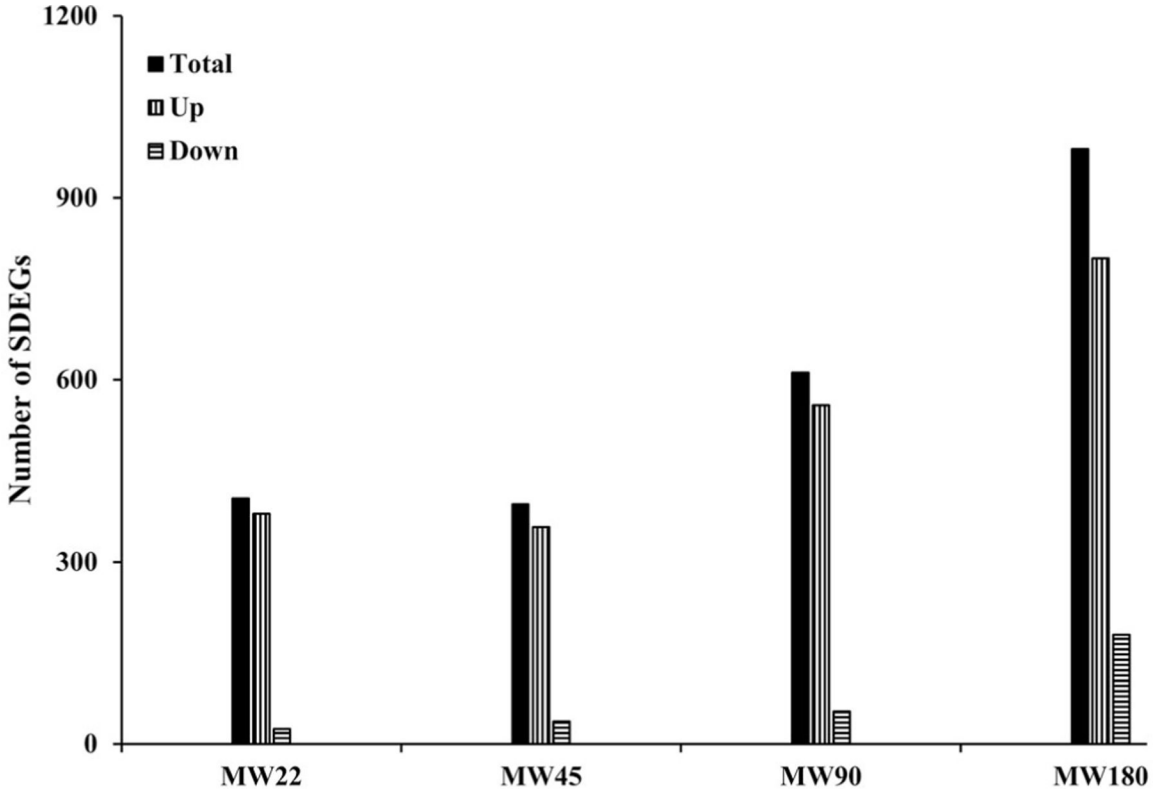

Figure 7.

Gene expression profile in rat lungs in response to exposure to MWCNT-7. Total RNA isolated from the control and MWCNT exposed lungs obtained from the euthanized rats was analyzed for global gene expression profile and the significantly differentially expressed (total, up-regulated, and down-regulated) genes were identified as described in the Materials and Methods section.

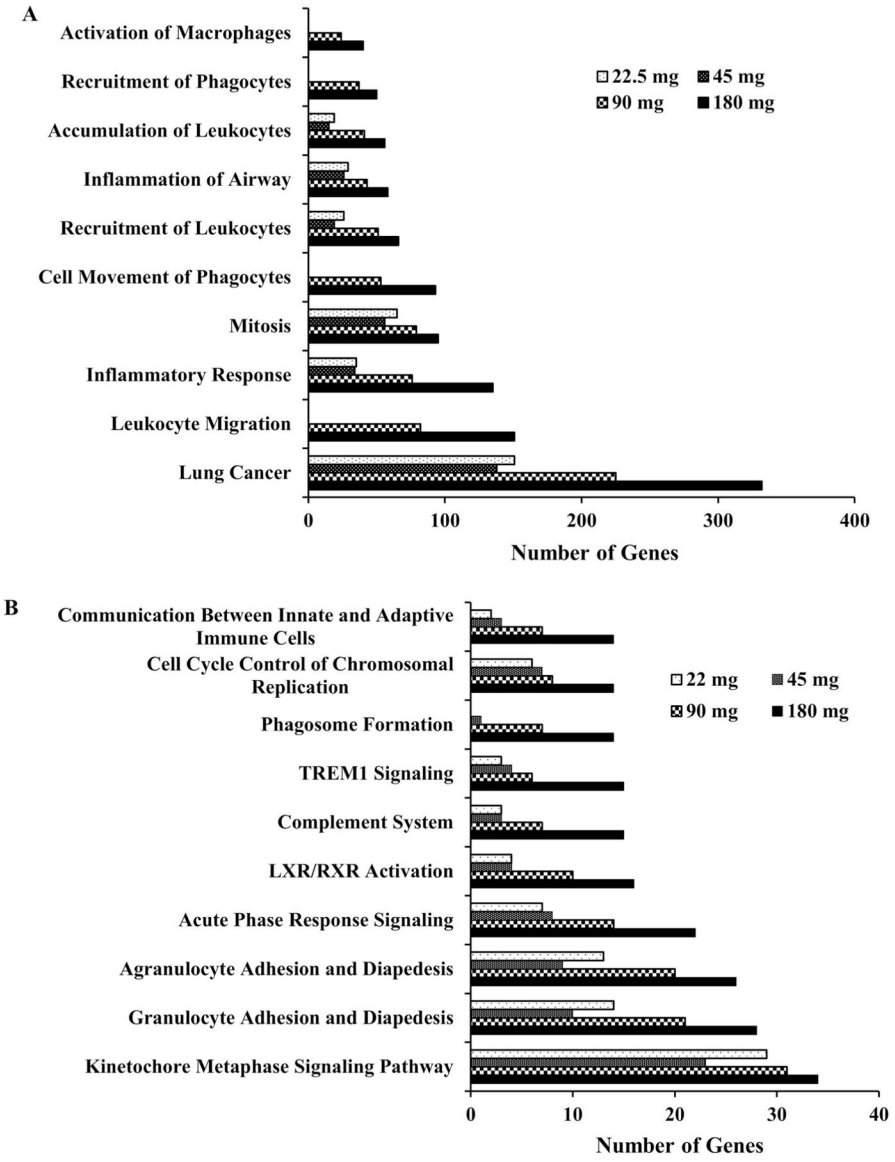

Figure 8.

Biological functions and canonical pathways enriched in the lungs of the rats. Total RNA isolated from the air or MWCNT-7 exposed lungs obtained from the euthanized rats were analyzed for global gene expression profile and the SDEGs were identified as described in the Materials and Methods section. The SDEGs were used as input in the Ingenuity Pathway Analysis program and the classification categories significantly enriched in response to MWCNT-7 exposure in the rats were identified. Ten of the significantly enriched biological functions (A) and canonical pathways (B) and the number of SDEGs belonging to those categories are presented.

Table 1.

Fold changes in gene expression in response to MWCNT-7 exposure in rats.

	MWCNT-7 Cumulative dose (mg/m^3)h			
Transcript	**22.5**	**45**	**90**	**180**
Recruitment of phagocytes, activation of macrophages, and phagosome formation				
C-C motif chemokine ligand 2 (Ccl2)	3.03	2.36	4.20	12.80
C-C motif chemokine ligand 7 (Ccl7)	3.34	2.41	6.25	11.91
C-C motif chemokine ligand 9 (Ccl9)	2.09	2.07	2.45	3.38
C-X-C motif chemokine ligand 2 (CXCL2)	2.45	3.05	2.35	3.37
Chemokine (C-X-C motif) ligand 3 (CXCL3)	1.12	1.24	1.27	1.50
Chemokine (C-X-C motif) ligand 6 (CXCL6)	4.65	3.97	4.88	9.40
C-X-C motif chemokine ligand 10 (CXCL10)	1.67	1.05	2.52	3.90
Resistin like alpha (RETNLA)	4.04	3.61	7.51	10.79
Selectin E (SELE)	2.54	1.45	3.51	5.31
Selectin P (SELP)	1.56	1.31	2.32	2.72
Inflammatory response				
Serum amyloid A-like 1 (SAAL1)	3.19	3.61	4.48	9.34
Orosomucoid 1 (ORM1)	2.72	22.31	5.36	16.43
Complement C1 (C1)	1.23	1.54	1.72	2.12
Complement C3 (C3)	1.88	2.21	2.27	2.99
Complement C6 (C6)	1.47	1.49	1.97	2.51
Complement C1q A chain (C1QA)	1.27	1.16	1.47	1.70
Complement C1q B chain (C1QB)	1.29	1.19	1.59	1.78
Complement C1q C chain (C1QC)	1.22	1.07	1.36	1.58
Complement factor B (CFB)	1.31	1.35	1.36	1.66
Integrin subunit alpha E (ITGAE)	−1.02	1.22	1.56	1.56
Integrin subunit alpha M (ITGAM)	1.27	1.43	1.99	2.47
Integrin subunit alpha X (ITGAX)	1.25	1.19	1.42	1.82
Integrin subunit beta 8 (itgb8)	1.41	1.63	1.80	2.12
Triggering receptor expressed on myeloid cells 1 (TREM1)	1.06	1.13	1.25	1.72
Toll-like receptor 1 (TLR1)	1.07	1.03	1.19	1.83

	MWCNT-7 Cumulative dose (mg/m^3)h			
Transcript	**22.5**	**45**	**90**	**180**
Toll-like receptor 5 (TLR5)	−1.02	1.33	1.10	1.93
Toll-like receptor 10 (TLR10)	1.03	1.03	1.19	1.83
Toll-like receptor 11 (TLR11)	−1.35	1.46	1.40	1.69
Toll-like receptor 12 (TLR12)	−1.01	1.56	2.23	2.16
Interleukin 1 beta (IL1b)	1.58	1.50	1.77	2.01
Colony stimulating factor 1 (CSF1)	1.24	1.19	1.51	1.74
CD86 molecule (CD86)	1.34	1.19	1.42	1.80
Hemopexin (HPX)	1.21	1.27	1.55	1.92
Low density lipoprotein receptor (LDLR)	1.10	1.29	1.41	1.69
Inter-alpha-trypsin inhibitor heavy chain 4 (ITIH4)	1.39	1.13	1.56	2.13
Oxidative stress response				
Superoxide dismutase 2 (SOD2)	1.73	1.75	1.99	2.65
NADPH oxidase organizer 1 (NOXO1)	2.19	2.26	2.48	3.37
Lactoperoxidase (LPO)	−1.56	−1.09	5.53	4.70
Heme oxygenase 1 (HMOX1)	1.24	1.20	1.16	1.53
Lipocalin 2 (LCN2)	3.05	4.24	4.17	6.22
Haptoglobin (HP)	1.62	1.64	1.74	2.67
Fibrosis				
Serpin family E member 1 (SERPINE1)	1.11	1.59	2.46	3.61
TIMP metallopeptidase inhibitor 1 (TIMP1)	1.33	1.25	1.59	1.81
Secreted phosphoprotein 1 (SPP1)	2.22	2.80	10.33	26.26
Matrix metallopeptidase 12 (MMP12)	1.59	1.41	2.33	5.97
Chitinase, acidic (CHIA)	3.95	3.76	4.68	4.83
Pentraxin 3 (PTX3)	2.12	1.48	2.21	2.88
Chitinase 3 like 1 (CHI3L1)	2.09	2.09	2.49	3.56
Cancer (cell cycle control)				
Cell division cycle 45 (CDC45)	1.44	1.76	1.36	1.91
Cell division cycle 6 (CDC6)	2.16	2.85	2.61	4.38
Cell division cycle 7 (CDC7)	1.11	1.26	1.33	1.57
Minichromosome maintenance complex component 2 (MCM2)	1.39	1.32	1.36	1.62

Inhal Toxicol. Author manuscript; available in PMC 2023 January 30.

	MWCNT-7 Cumulative dose (mg/m^3)h			
Transcript	**22.5**	**45**	**90**	**180**
Minichromosome maintenance complex component 3 (MCM3)	1.45	1.47	1.43	1.75
Minichromosome maintenance complex component 4 (MCM4)	1.21	1.25	1.31	1.65
Minichromosome maintenance complex component 5 (MCM5)	2.49	1.89	2.41	3.29
Minichromosome maintenance complex component 6 (MCM6)	1.57	1.47	1.57	2.07
Origin recognition complex, subunit 1 (ORC1)	2.15	2.16	2.97	3.31
Origin recognition complex, subunit 6 (ORC6)	1.22	1.21	1.23	1.51
Cancer (kinetochore metaphase)				
Aurora kinase B (AURKB)	1.64	1.91	1.99	1.77
Baculoviral IAP repeat-containing 3 (BIRC3)	1.31	1.17	1.87	1.71
Baculoviral IAP repeat-containing 5 (BIRC5)	2.71	1.81	1.96	2.49
BUB1 mitotic checkpoint serine/threonine kinase (BUB1)	1.58	1.91	1.85	2.33
BUB1 mitotic checkpoint serine/threonine kinase B (BUB1B)	2.28	2.34	2.14	2.92
Cyclin B1 (CCNB1)	2.59	2.37	2.71	4.29
Cyclin-dependent kinase 1 (CDK1)	3.07	2.47	2.77	3.06
Centromere protein A (CENPA)	3.07	2.47	2.77	1.97
Centromere protein E (CENPE)	2.11	2.19	1.83	2.61
Centromere protein K (CENPK)	1.90	1.82	2.13	3.00
Centromere protein T (CENPT)	2.05	1.64	2.10	2.52
Centromere protein U (CENPU)	2.87	2.17	2.39	3.57
Centromere protein W (CENPW)	3.49	2.07	2.86	4.33
Extra spindle pole bodies like 1, separase (ESPL1)	1.84	1.80	1.76	2.41
Kinetochore associated 1 (KNTC1)	1.93	1.64	2.07	3.26
Microtubule associated serine/threonine kinase-like (Mastl)	2.37	2.37	2.10	3.08
NDC80 kinetochore complex component (NDC80)	2.22	1.39	2.63	2.39
NUF2 component of NDC80 kinetochore complex (NUF2)	2.29	1.72	2.98	3.03
Polo-like kinase 1 (PLK1)	2.34	2.00	2.10	2.66
Polyamine-modulated factor 1 (PMF1)	1.30	1.18	1.12	1.71
PTTG1 regulator of sister chromatid separation, securin (PTTG1)	2.57	1.84	2.84	2.90
Spindle and kinetochore associated complex subunit 1 (SKA1)	2.77	2.63	2.60	3.28
Spindle and kinetochore associated complex subunit 3 (SKA3)	1.96	1.60	2.17	2.38

Inhal Toxicol. Author manuscript; available in PMC 2023 January 30.

	MWCNT-7 Cumulative dose (mg/m^3)h			
Transcript	**22.5**	**45**	**90**	**180**
SPC25 component of NDC80 kinetochore complex (SPC25)	2.06	2.39	2.54	3.13
Ttk protein kinase (TTK)	2.77	1.61	2.05	2.96

The fold changes in gene expression in the MWCNT-7 exposed rat lungs, compared to the corresponding controls, are presented. Categorization of the genes into the various groups is based on the results of the IPA analysis. The same gene may belong to more than one IPA functional category. However, each gene is presented in only one category in the table.